Journal of MATERIALS RESEARCH

Review
DOI: 10.1557/jmr.2019.329

*This section of Journal of Materials Research is reserved for papers that are reviews of literature in a given area.*

ATOMIC LAYER DEPOSITION FOR EMERGING THIN-FILM MATERIALS AND APPLICATIONS

FOCUS ISSUE

# Atomic layer–deposited nanostructures and their applications in energy storage and sensing

Zhe Zhao[1], Ye Kong[1], Zhiwei Zhang[1], Gaoshan Huang[1], Yongfeng Mei[1,a)]

[1]*Department of Materials Science, Fudan University, Shanghai 200433, People's Republic of China*

[a)]Address all correspondence to this author. e-mail: yfm@fudan.edu.cn

Received: 8 September 2019; accepted: 2 October 2019

**Nanostructures are considered to have great potential and are widely used in energy storage and sensing devices, and atomic layer deposition (ALD) is of great help for better nanostructure fabrications. ALD can help to preserve the original properties of materials, and, meanwhile, the excellent film quality, nanoscale precise thickness control, and high conformality also play important role in fabrication process. To enhance the performance of energy storage and sensor devices, ALD has been used in directly fabricating active nanostructures, depositing protective passivation layers, etc. ALD is a convenient technique which has been widely engaged in energy-related fields including electrochemical conversion and storage, as well as in sensor and biosensors. The related research interest is increasing significantly. In this review, we summarize some of the latest works on ALD for batteries, supercapacitors, and sensors, and demonstrate the benefits of ALD comprehensively. In these devices, different materials are deposited by ALD under different conditions to achieve better battery performance, higher supercapacitor capacitance, and higher sensitivity. This review fully presents the strengths of ALD and its application in energy storage and sensing devices and proposes the future prospects for this rapidly developing technology.**

## Introduction

With the development of society, demands for new materials applied in energy- and sensor-related area have become more and more urgent [1, 2]. The concept of "nanostructure" was first proposed in 1959 [3], and has become one of the most promising materials because of their nanoscale properties and high controllability. The materials with nanostructures have one or three dimensions in the scale of 1–100 nm [4, 5]. Hierarchical nanostructured materials are composites comprised with various functional phases and interfaces [6, 7, 8, 9]. In the resultant hierarchical nanomaterials, combination of different phases with electrical/magnetic/mechanical/optical functions leads to new properties that cannot be found in conventional materials [10, 11, 12, 13]. However, the fabrication of composite structure through the combination of functionalized phases or confined different nanomaterials in space of few nanometers is still very challenging [14]. One of the challenges in the fabrication of novel nanostructures is the direct manipulating of atoms, which can preserve the properties of both nanomaterials when combining those to form a new composite structure [15, 16, 17, 18]. One common strategy for constructing composite structures is the deposition of nanoparticles or monolayers on the surfaces of substrates [19]. Various deposition approaches, such as solution-based precipitation [20], sol–gel method [21], layer-by-layer (LBL) deposition [22], electrodeposition [23], chemical vapor deposition (CVD) [24], and atomic layer deposition (ALD) [19], have been explored. Among all the deposition methods, ALD is one of the most promising deposition techniques due to good conformality, excellent thickness and composition controlability, and ability of manipulation at atomic scale [25, 26], and therefore has become a promising technique in nanostructure fabrications. In ALD-related researches, a wide range of materials and structures such as various wafers [27], nanoparticles [28], nanowires [29], nanotube [30], soft materials [31], and biological materials [32], can be served as substrates for ALD coating. The resultant nanostructures are applied for enhanced performance in batteries [33, 34], supercapacitors [35, 36, 37], catalysts [38, 39, 40], and sensor areas [41, 42].

Along this review article, the function and the applications of ALD will be discussed. The first part of the article illustrates the history and advantages of ALD, focusing on its function for nanostructure fabrication. Then, the applications in supercapacitor and battery will be demonstrated. Sensor and especially biosensor applications of ALD-fabricated nanostructures are subsequently summarized. Finally, the outlook and conclusion will describe the perspectives and challenges of ALD method in terms of nanostructure fabrication and processing.

## History and advantages of ALD

ALD is a technique enabling a variety of thin film materials coating from the vapor phase [6, 43]. ALD was first invented by Finland physicist Tuomo Suntola in 1977, which was called atomic layer epitaxy (ALE) [19]. Depositions of ZnS, $SnO_2$, and GaP layers through vapor phase on glass plate were achieved via this method [44, 45, 46]. In the next decades and up to now, the synthesis strategy was then referred to as ALD [47]. A typical ALD cycle consists of two gaseous chemical precursors that perform self-limiting reactions with each other on certain substrates and one precursor is firstly pulsed into the reactor chamber to adsorb on the surface of substrate under vacuum [48, 49]. The reactions between precursors and active groups on the substrate are self-limiting, whereas the surplus precursor molecules and the intermediate products are removed by inert carrier gas purging (commonly $N_2$ or Ar) [49]. Only one monolayer is generated on the surface of substrate eventually. The next step involves the purging of a second chemical precursor gas to react with the molecules coating on substrate to form the resultant layer [50, 51, 52, 53]. Subsequently, after purging of carrier gas again, the untreated precursors and intermediate products are removed. Therefore, only one monolayer of desired material is deposited on the substrate in one cycle and the thickness of obtained film/membrane can be well controlled by tuning the number of cycles [54, 55].

The major advantage of ALD is the controllability at atomic scale control due to its sequential, self-saturating, vapor phase reaction [28, 56, 57]. Compared with other deposition techniques, the conformality of nanomembrane deposited via ALD is the crucial feature [58, 59, 60]. The unique characteristic broadens its applications in decorating and modifying three-dimensional structures. With sufficient waiting times of precursors pulsing, the precursor can penetrate into deep structure, leading to complete membrane coating on the entire surface [61]. On the other hand, sequential deposition induces the uniform growth on various structures, whereas other deposition techniques, for example, CVD, may hardly generate such uniform layer due to rapid surface reactions and shadowing effects [62]. In a typical ALD cycle, only finite surface sites can be adsorbed, and therefore the reactions only produce a finite number of surface species. The self-limiting reaction between precursors can produce a thin layer at atomic level control in a sequential deposition process. Thus, an apparent advantage of ALD is the highly controllable of thickness when depositing membranes. Through the regulation of cycling number of ALD process, the thickness of film can be tailored. In the single depositing process, ultrathin layer with thickness about or even less than 1 Å can be fabricated [63]. In addition, composition control is another obvious advantage of the ALD technique [64, 65, 66]. Composition control has been illustrated with a variety of materials such as zinc oxide (ZnO), aluminum oxide ($Al_2O_3$), or titanium dioxide ($TiO_2$), and others [42, 67, 68, 69]. These membranes can be deposited and compositionally controlled via precursors choosing in ALD process. For example, to produce multiple nanostructures with ZnO and $Al_2O_3$ composite layer, the component of resultant membrane can be adjusted through changing the cycle ratios between ZnO and $Al_2O_3$ [70, 72, 73], which can regulate and combine various properties of the materials such as conductive performance [74, 75], pseudocapacitive property [76], or optical characteristic [77]. Figure 1 shows a collection of electron microscopy images of nanostructures, in which ALD was used in at least one of the fabrication steps.

Because of its unique advantages, ALD technique may play an essential role in energy storage and sensing fields. Herein, we summarize the concrete function of this method via selective examples. We will focus on the applications in supercapacitors, batteries, and sensors (including biosensors). Our reviews on the applications of ALD for nanostructures are summarized as follows:

### Growth and deposition of active materials

Because of the strong combination between ALD coatings and substrate, active materials can be directly deposited as functional body on certain substrate with good characteristic. The active materials include uniform nanomembrane or nanoparticle, which can provide desired properties like high catalytic activity, good conductivity, outstanding capacitance, or bio compatibility [78, 79, 80]. Such applications commonly involve a one-pot synthesis via ALD deposition, which is convenient and efficient [28, 80]. The quantity and morphology of active materials are also simple to control through adjusting the deposition process, and it is easy to establish the relation between structure and property.

### Formation of the protective layer

The uniform and firm films can be used as a protective layer to separate active component and harsh environment. For example, the corrosion from electrolyte will degrade the

https://doi.org/10.1557/jmr.2019.329 Published online by Cambridge University Press

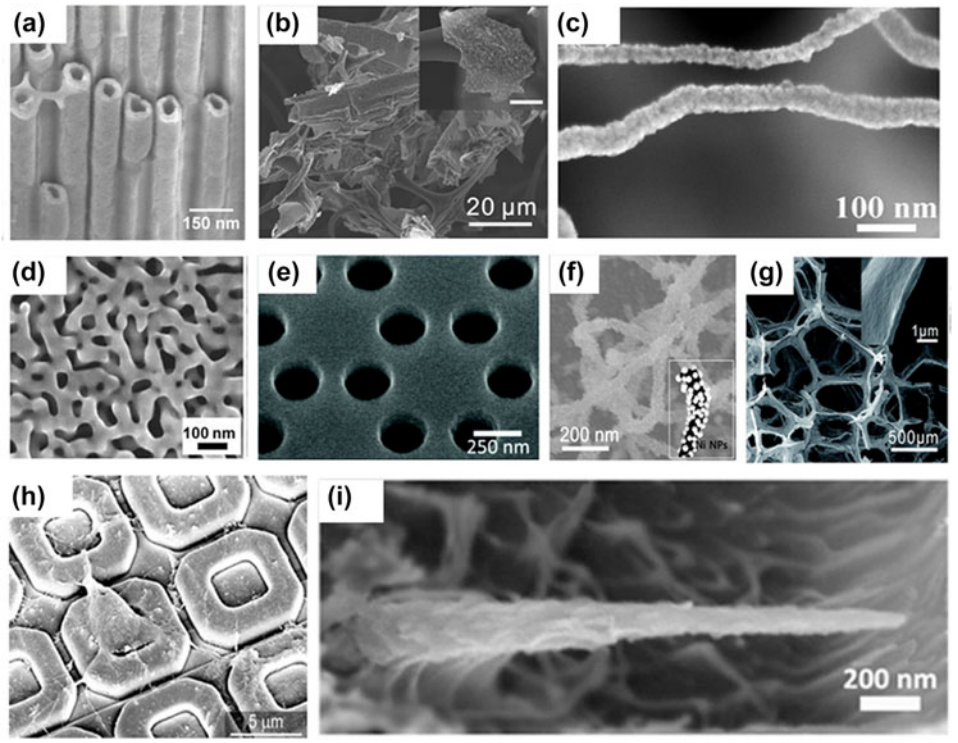


**Figure 1:** Complex nanostructures synthesized by ALD. (a) Pt nanotube structure observed inside porous anodic alumina template cross-section. Adapted from Ref. 141. (b) ZnO nanomembrane obtained with 200 ALD cycles. The inset shows the ZnO nanomembranes in a vial. Adapted from Ref. 150. (c) CNT@$Co_3O_4$ on CC. Adapted from Ref. 127. (d) Nanoporous gold films after CoO deposition. Adapted from Ref. 136. (e) 2D honeycomb lattice photonic crystal fabricated in an air-bridge format. Adapted from Ref. 138. (f) Ni grown on CNTs after 250 cycles of ALD (as illustrated in the inset). Adapted from Ref. 135. (g) C/ZnO porous network of the sample after pyrolysis. Adapted from Ref. 79. (h) Rat cortical neuron on the sensor input structure of a CMOS FG FET chip, which was passivated by an $Al_2O_3$/$HfO_2$ multilayer. Adapted from Ref. 81. (i) Conical $Al_2O_3$ replicas obtained by coating the conical nanochannels by 150 cycles of ALD $Al_2O_3$. Adapted from Ref. 139.

electrochemical performance of electrode, whereas ALD coatings can prevent the structure from destroying [81, 82]. In addition, the nanomembrane can efficiently reduce the dissolution of active materials [83]. In the biosensor-related field, maintaining the characteristic stability of biologic active molecule such as enzyme, antibody, biotin, and certain proteins is especially critical [84, 85, 86]. The protective shell formed by the ALD technique has become a promising strategy.

### Direct establishment of nanoarchitecture

ALD technique can participate in the establishment of nanoarchitecture, owing to its fascinating conformal depositing advantage. For example, one may utilize area selective ALD deposition to generate certain pattern or step [82, 87], and nanoarchitectural materials can be elaborated by ALD [79, 88, 89, 90]. During the vapor phase penetration, nanomembrane can form in deep channel of substrate, which broadens the applications of ALD technique from two-dimensional plate to three-dimensional framework. On the other hand, the substrates of ALD coatings can also be used as sacrificial templates to produce self-standing layer [91, 92].

## Applications of ALD in batteries

Batteries, which are considered as successful and promising energy storage devices for the future development, such as lithium-ion batteries (LIBs), lithium–sulfur batteries (LSBs), sodium-ion batteries (NIBs), and zinc–air batteries [93, 94, 95, 96, 97] have been deeply investigated in mechanism, materials, and applications, owing to their high energy capacity, excellent storage density, low-self discharging, splendid stability, and so forth [98, 99, 100]. Nevertheless, even the state-of-the-art batteries currently suffer the insufficiency in the demand of high charging-discharging rate, critical safety of the batteries, low cost, and environment-friendly properties along with the progress of the technology. It is widely believed that the introduction of nanostructure could be an efficient route to solve the issues [101, 102]. However, highly controllable fabrication of nanostructures as well as atomic scale manipulation are still challenging. More and more researches are concentrating on the precise controllable nanomembrane-like structures and this may provide new insight to overcome the challenges of the modern energy storage devices.

Tremendous researches on ALD have been performed in the energy storage systems, whereas some notable achievements

https://doi.org/10.1557/jmr.2019.329 Published online by Cambridge University Press

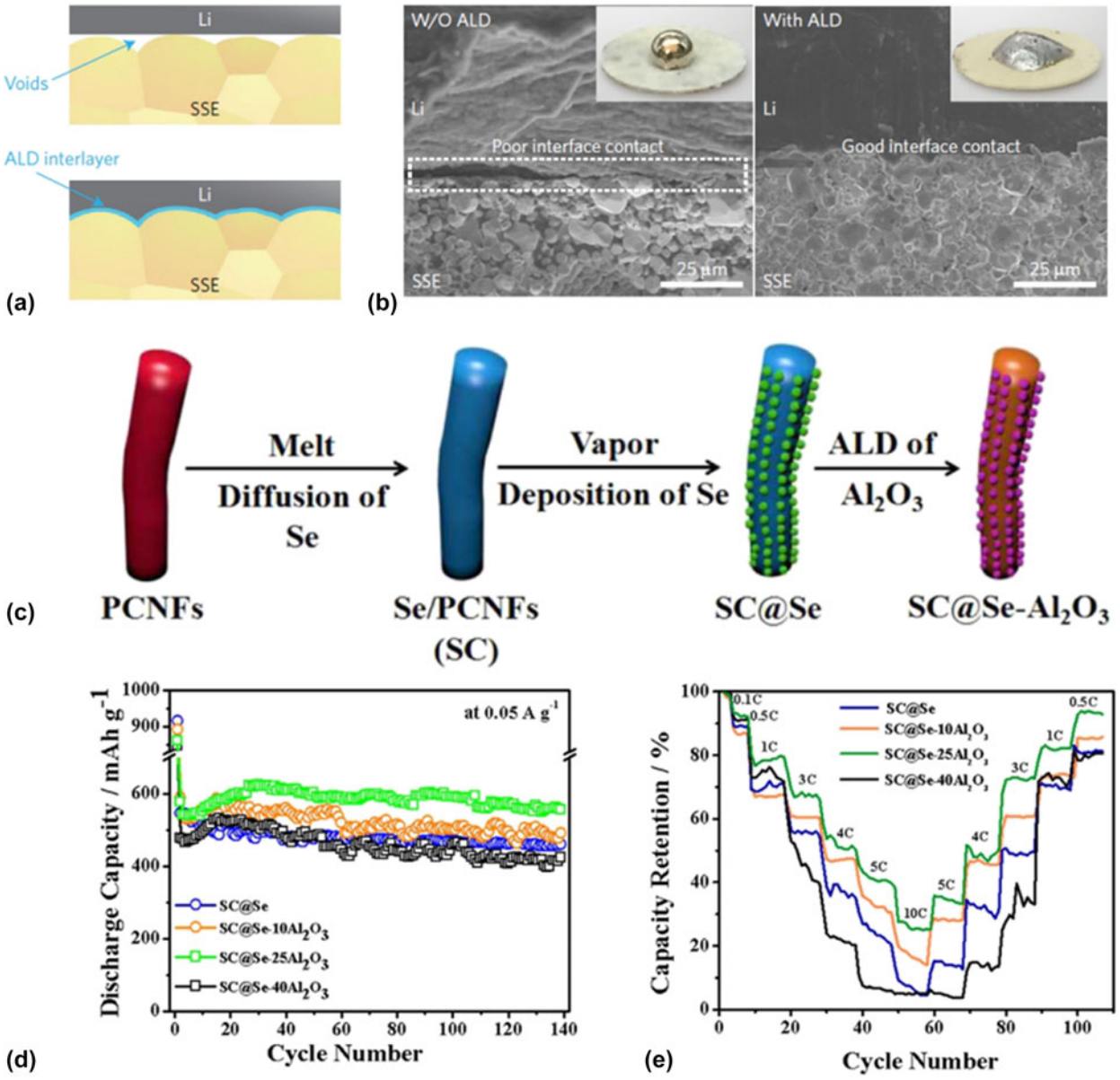


**Figure 2:** (a) Schematic of the wetting behavior of garnet surface with molten Li. (b) SEM images of the garnet solid-state electrolyte/Li metal interface. Without the ALD-$Al_2O_3$ coating, garnet has a poor interfacial contact with Li metal even on heating. With the help of ALD–$Al_2O_3$ coating on garnet, Li metal can uniformly bond with garnet at the interface on heating. Inset are photos of melted Li metal on top of the garnet surface clearly demonstrating classical wetting behavior for the ALD-treated garnet surface. (a) and (b) are adapted from Ref. 104. (c) Schematic illustration of the preparation process for SC@Se–$x$$Al_2O_3$ composites. (d) Cycle stability of SC@Se–$x$$Al_2O_3$ composites. (e) Comparison of the rate capability of SC@Se–$x$$Al_2O_3$ composites expressed as a percentage of the initial capacity at 0.1 C. (c)–(e) are adapted from Ref. 102.

have been obtained in the past decades. For example, Snyder et al. [101] firstly used ALD TiN to improve the LIB charge–discharge performance and keep the batteries maintaining a constant charge capacity with a value close to the theoretical value by tailing the interface between the anode and the liquid electrolyte which induce to the removal of surface carbonate species and the avoidance of the anode corrosion by the electrolyte. The TiN fabricated by ALD in the study acted as a nanostructure layer for blocking the decomposition of the $Li_4Ti_5O_{12}$ anode. Besides, Li et al. [33] deposited $SnO_2$ onto the graphene nanosheets by ALD which could facilely manipulate the morphology and the crystallinity of the $SnO_2$ layer and got a conductive and flexible hybrid structure simultaneously. By controlling the ALD parameters, they found that the amorphous $SnO_2$ composite showed a better cycling stability than the crystallization $SnO_2$ composite because of its isotropic property. In this study, ALD technique was utilized to directly synthesize the anode active material by which the structure phase of the anode layer can be precisely controlled. What's more, the ALD membranes could also provide a significant

https://doi.org/10.1557/jmr.2019.329 Published online by Cambridge University Press

protection of the electrodes from erosion by the various electrolytes. For instance, the conformal ultrathin $Al_2O_3$ layer constructed by ALD was coated outside the natural graphene which can protect the surface of the electrodes while keeping a smooth pathway for electronic transferring, which induced both long-term durability and safety of the batteries. Here we refer some cross-sectional works to review the progress of the employment of the ALD in batteries field in the following sections.

## ALD for structure engineering/modification layer

To improve the comprehensive performance of the batteries, commonly a well-designed structure is needed. ALD is capable to construct an intermediate layer or auxiliary medium for the nanostructure engineering of the entire battery system including the anode, the cathode, the electrolyte, the separator, and especially the interfaces between them. For instance, the giant interfacial impedance of lithium/garnet-type electrolyte in garnet-type solid-state electrolyte Li batteries had block the development of this environment stable, efficient, and promising storage devices for a long time. Hu et al. [103] found that the ultrathin $Al_2O_3$ membrane could effectively negate the interfacial impedance between the metal lithium and the garnet electrolyte for its decreased sintering temperature and increased lithium ion conductivity. As shown in Figs. 2(a) and 2(b), they modified the garnet surface with 40 ALD cycles of $Al_2O_3$ coating [104]. They found that the $Al_2O_3$ layer could help the molten Li conformally to coat the surface without void space, which can be distinctly observed in the SEM images in Fig. 3(b) that the $Al_2O_3$ layer enhances the contact between the garnet and the metal Li. The impedance of the obtained ALD-modified interfacial layer showed a relatively low value of 1 $\Omega$ cm$^2$ compared with 1710 $\Omega$ cm$^2$ of the non-ALD samples at room temperature. They ascribed the improvement of the performance to the wetting of metal lithium in contact with the garnet electrolyte and the efficacious lithium ion transport through the interfacial layer offered by the ALD $Al_2O_3$. Another case is that the atomic layer $Al_2O_3$ was utilized to construct stable freestanding carbon–selenium cathodes which exhibited a high mass loading of selenium as well as superior cyclic performance.

Zhang and his coworkers fabricated a selenium composite cathode material by vapor depositing Se onto porous carbon

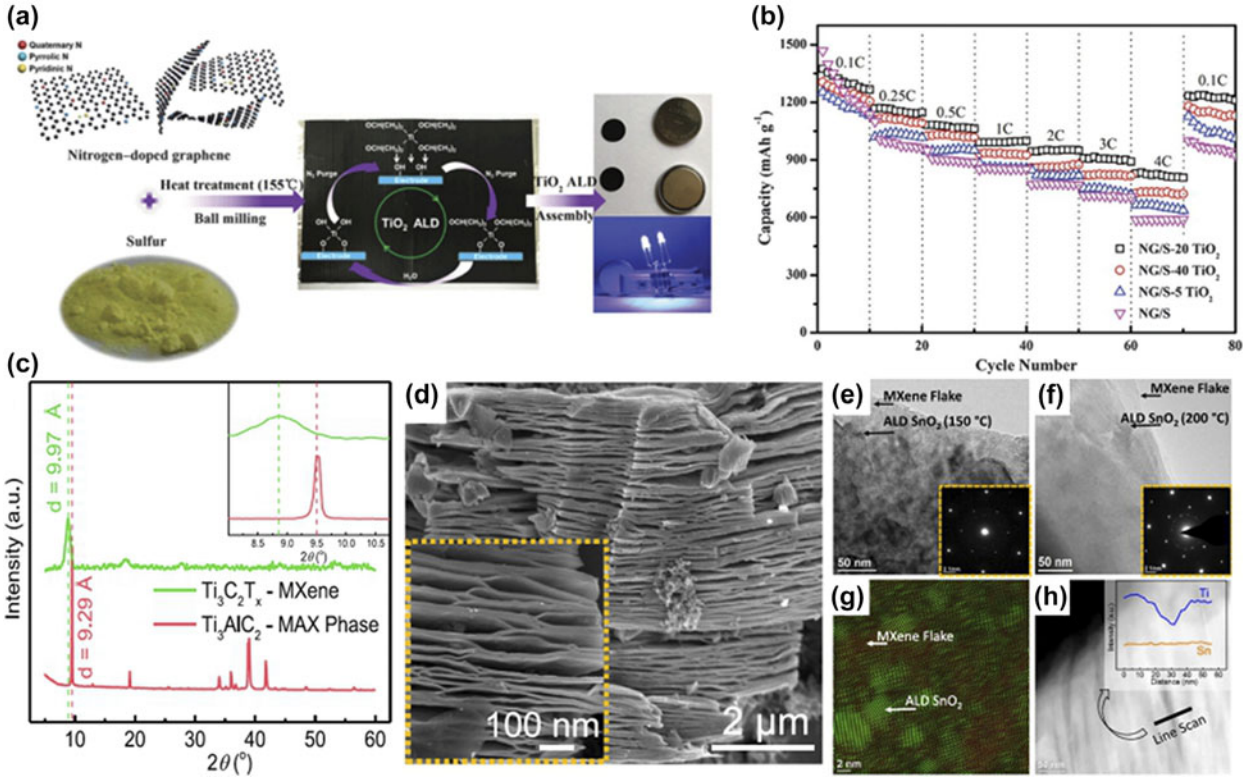


**Figure 3:** (a) Schematic illustration of the NG/S–$TiO_2$ preparation process and the experimental demonstration showing that the battery can light up two blue LEDs. (b) The rate performances of the electrodes at various current densities. (a) and (b) are adapted from Ref. 109. Characterization of as-prepared HF-etched $Ti_3C_2$ MXene: (c) XRD patterns of $Ti_3AlC_2$ and $Ti_3C_2$. (d) Typical SEM image of HF-etched $Ti_3C_2$ Mxene. TEM analysis of MXene sheets coated with a 50 nm-thick layer of $SnO_2$: low-magnification TEM image and SAED pattern for ALD (e) at 150 °C and (f) at 200 °C. (g) Fourier-filtered high-resolution RGB image for ALD at 200 °C, showing the presence of two phases and (h) STEM image along with the EDS line-scan for ALD @150 °C showing the conformal $SnO_2$ coating. (c)–(h) are adapted from Ref. 110.

https://doi.org/10.1557/jmr.2019.329 Published online by Cambridge University Press

nanofiber mats and subsequently ALD of $Al_2O_3$ with the synthesis routine shown in Fig. 2(c) [102]. They firstly introduced the ALD technique into the Se batteries and systematically investigated the effect to the electrochemical properties of the batteries induced from the $Al_2O_3$ thickness that is precisely controlled by the ALD. A 67 wt% of Se content correspondingly provided by 25 cycles $Al_2O_3$ layers shows an excellent cyclic stability which can deliver specific capacity of 503.5 mA h/g after 1000 cycles at 0.5 A/g and even maintain 72.1% of the capacity comparing to the original with analysis details shown in Figs. 2(d) and 2(e). They contributed the enhancement of the performance to the exceptional conductivity, fast ionic/charge transfer, limitation of the dissolution of the sodium polyselenides, and the confinement of the volume expansion during charging/discharging.

Moreover, Hwang et al. [105] build a flexible connection via the combination of ALD $Al_2O_3$ between the Si anode and the additive vinylene carbonate (VC), which remarkably led to an increasement of performance from a 73 to 11% capacity loss. Additionally, some other materials such as titanium oxide ($TiO_2$), tin oxide ($SnO_2$), and even the garnet $Li_7La_3Zr_2O_{12}$ (LLZO) also have been deposited to optimize the lithium batteries performance serving as a structure modification layer [106, 107, 108].

## ALD for active electrode materials

Direct implementation of ALD on the synthesis of electrode materials may also provide an insight to the design of novel batteries. Because of the great capability to form conformal and thickness-controlled membranes, ALD emerges as an ideal technique to fabricate anode or cathode materials that can basically determine the specific capacity, durability, and other electrochemical performance of the batteries. A typical example is that Wang and coworkers fabricated a sandwich-like structure media as a cathode for Li–S battery using N-doped graphene (NG), sulfur, and ALD–$TiO_2$ as raw materials [109]. As the details shown in Fig. 3(a), $TiO_2$ was deposited on the NG-pure sulfur composites that are used as a conductive matrix and the source of elemental S. Two LED bulbs can even be lightened by the assembled battery using the composite as raw materials. Various cycles of ALD here for 0, 50, 20, and 40 were adopted to investigate the effect of the ALD thickness to the performance. The obtained hybrid active material showed robust and steady architectures, which induced to the great improvement of the results as the NG/S–20$TiO_2$ could deliver 1374 mA h/g at 0.1 C for discharge capacity and keep an average coulombic capacity efficiency of approximately 99.7% at 1 C [see in Fig. 3(b)]. Ahmed et al. [110] proposed a methodology that oxide anodes can be grown on two-dimensional titanium carbide sheets (MXenes) through the ALD [XRD patterns, SEM, and TEM images shown in Figs. 3(c)–3(h)]. They deposited atomic layered $SnO_2$ up to the MXene, which showed an excellent electrochemical performance working as anodes for LIBs. Similarly, some other recent works on ALD $SnO_2$ were also studied by using various conductive substrates such as graphene nanosheets and carbon nanotubes for electrodes of batteries [111]. In summary, ALD has provided a good venue to build ideal electrode materials with excellent inner electrochemical performance and external controllable physical properties. However, most of the anode or cathode materials still suffer the deterioration during working process which has attracted the attention of the researchers.

Recently, Zhao and coworkers made a multilayer structure comprising two porous C layers and one sandwiched active ZnO (CZC) nanosheet [79], and the fabrication details and the corresponding characterizations are presented in Figs. 4(a)–4(d). In this composite, the thickness of the interlayer zinc oxide was accurately controlled by the ALD, which was used to investigate the effect of the thickness between the ZnO and the carbon coating. They found that the battery could perform a high capacity of 300 mA h/g at 5000 mA/g with the ratio of ZnO/C at about 1:1. The critical thickness ratio was proposed because the carbon layer is found fragile when the interlayer is thicker than the critical value which may ruin the stable SEI layer and reduce the conductivity. Additionally, ALD ZnO was also fabricated on expanded graphite (EG) as a binder-free anode for LIBs by Li and his coworkers [112] with the details shown in Figs. 4(e)–4(h). The composite was pressed into both self-supporting and flexible film and thus was directly utilized as anode. The ALD-ZnO/expanded graphite (ZG) anode battery shows a high stable capacity without using any conductive agent, binder, and current collector.

## ALD for the passivation layer

There is a well-known challenge that the dissolution or the side reactions of the active electrode materials in the electrolyte could seriously affect the cycling performance of the batteries [113]. One aspect to ameliorate the situation we discuss here is the achievement which has been obtained by constructing an ALD passivation/protection layer onto the active materials. One typical example is that Alexander and his coworkers proved that ALD $Al_2O_3$ can effectively protect the Li metal from corrosion [57]. The electrode was used as an anode for Li–S batteries to investigate the function of the ALD coating and they found that 14 nm ALD $Al_2O_3$ could alleviate the first cycle capacity loss because the ALD layer protected metal anode from the erosion of both the sulfur species and the electrolyte [see Fig. 5(a)]. As exhibited in Fig. 5(b), the great electrochemical performance with a 14-nm ALD $Al_2O_3$ coating can be clearly observed. Recently, Zhang's group used ALD

https://doi.org/10.1557/jmr.2019.329 Published online by Cambridge University Press

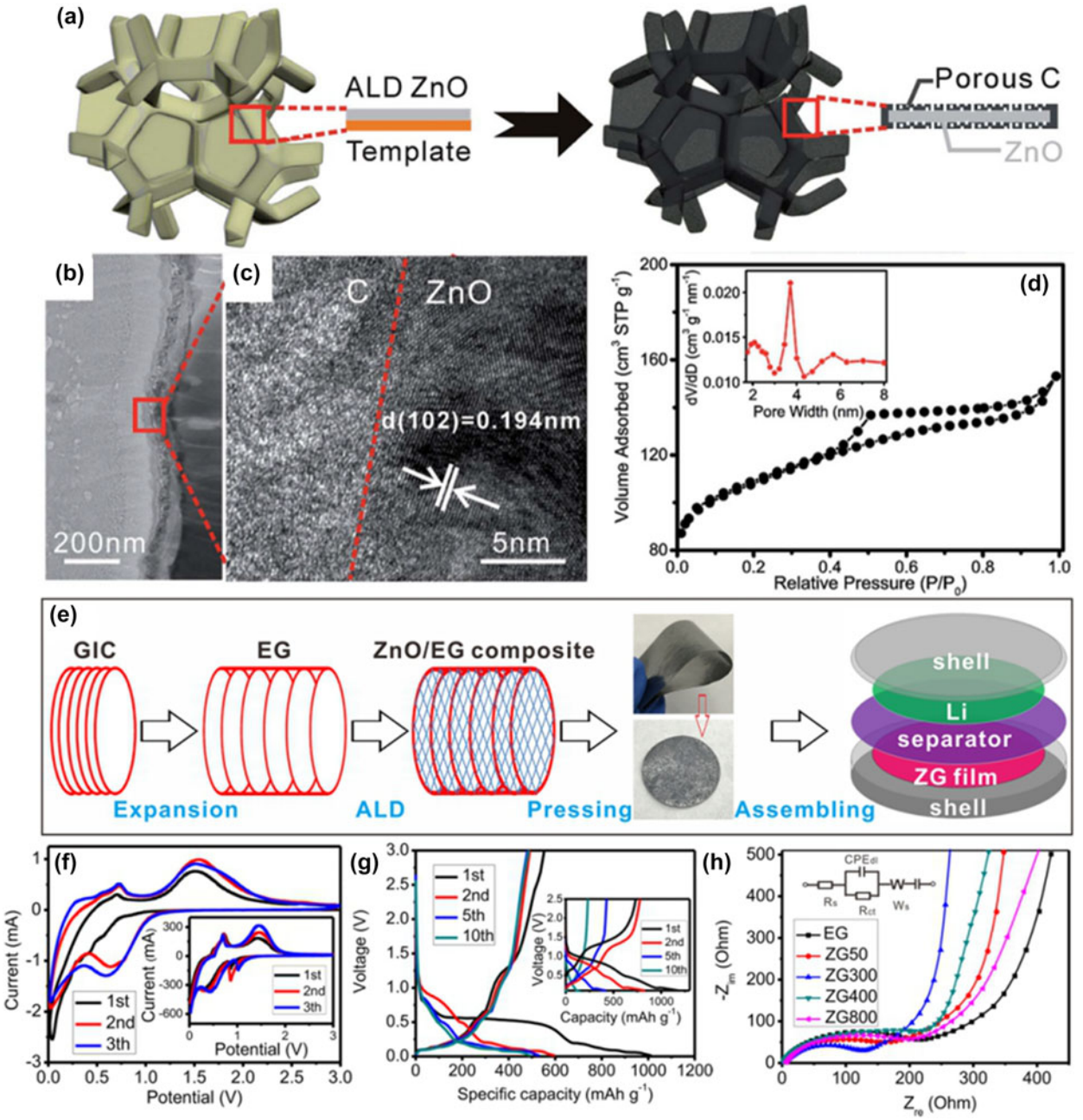


**Figure 4:** (a) Schematic of the synthesis procedure of CZC nanosheets. SEM images demonstrating the change of the electrode structure before and after 200 discharge/charge cycles. (b) Cross-sectional TEM image of a CZC nanosheet. The nanosheet is composed of a sandwiched structure. (c) High-resolution TEM image of the C/ZnO interface. (d) Nitrogen adsorption–desorption isotherms and pore size distribution (inset) of the CZC nanosheet sample. (a)–(d) are adapted from Ref. 79. (e) Schematic diagram of ZG preparation and corresponding device assembling. (f) CV curves of anode made from ZG300 (first three cycles) at 0.2 mV/s. The inset shows corresponding CV results from pure ZnO anode for comparison. (g) The 1st, 2nd, 5th, and 10th discharge and charge curves of ZG300 and pure ZnO (inset) at a current rate of 200 mA/g; (h) EIS of anode made from EG and ZG composites before galvanostatic discharging/charging cycles. The inset shows the equivalent circuit used to fit the experimental results. (e)–(h) are adapted from Ref. 112.

$TiO_2$ to protect the flexible C/S/$BaTiO_3$ electrode (CSB@$TiO_2$) for room temperature Na–S batteries which also provide a novel case for the ALD passivation layer on batteries [114]. In the work, they developed a tactic to synthesize a hybrid consisted of porous freestanding C mats, 3 wt% ferroelectric $BaTiO_3$ nanoparticles, and thickness-controlled $TiO_2$ [see Fig. 5(c)]. Corresponding TEM images and digital photos are shown in Fig. 5(d), respectively. They found that the ALD-modified electrode exhibited an excellent durability of remaining 382 mA h/g after 3000 cycles with a coulombic efficiency of 106.1% based on the 2nd cycle at 2 A/g. It is concluded that the function of $TiO_2$ passivation layer could inhibit the volume

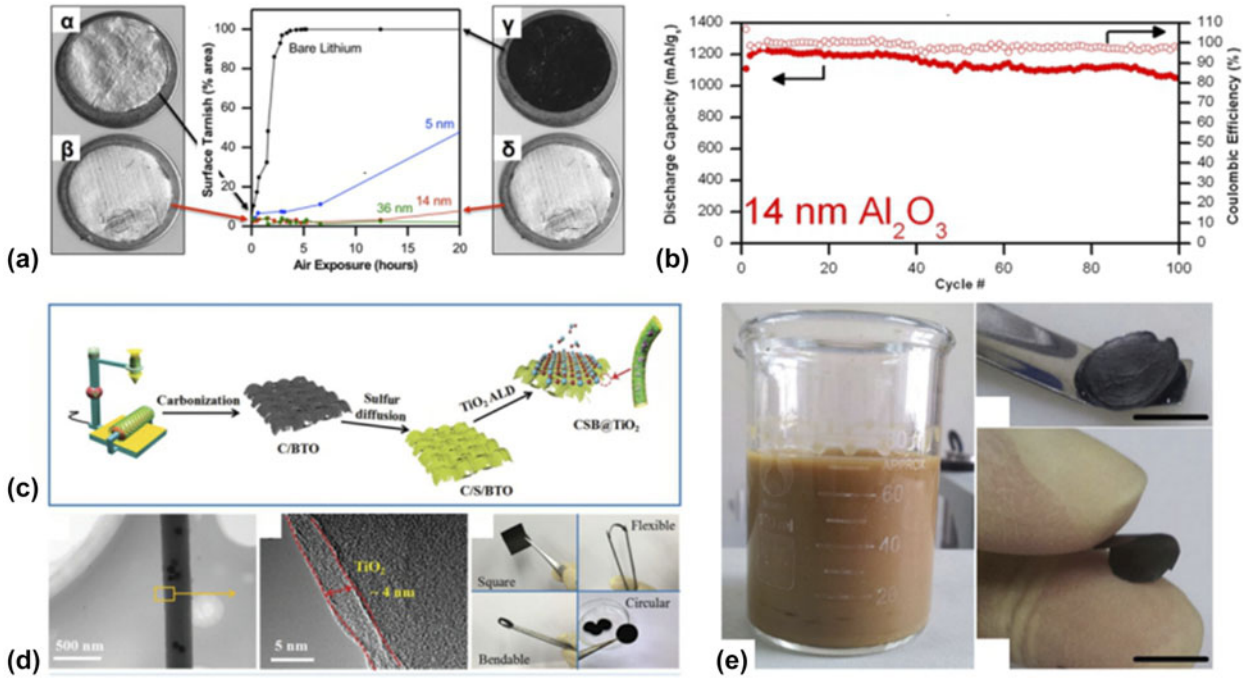


**Figure 5:** (a) Optical analysis of lithium foil surface tarnishing during atmospheric exposure at 25 °C and 40% relative humidity. (α) unprotected and (β) 14 nm ALD $Al_2O_3$-protected Li metal foil immediately upon removal from an argon atmosphere (γ) Bare and (δ) 14 nm ALD $Al_2O_3$-protected Li metal foil after 20 h exposed to atmosphere at 25 °C and 40% relative humidity. (b) anode protected with 14 nm ALD $Al_2O_3$ LiS cells. (a)–(e) are adapted from Ref. 57. (c) Schematic illustration of the CSB@$TiO_2$ electrode preparation process. (d) TEM images of the CSB@$TiO_2$ nanofiber and photograph of the CSB@$TiO_2$ freestanding electrode. (c) and (d) are adapted from Ref. 114. (e) Digital images of GO–S dispersion, as-obtained G–S hydrogel and a bent G–S aerogel. Scale bars, 1 cm. Adapted from Ref. 115.

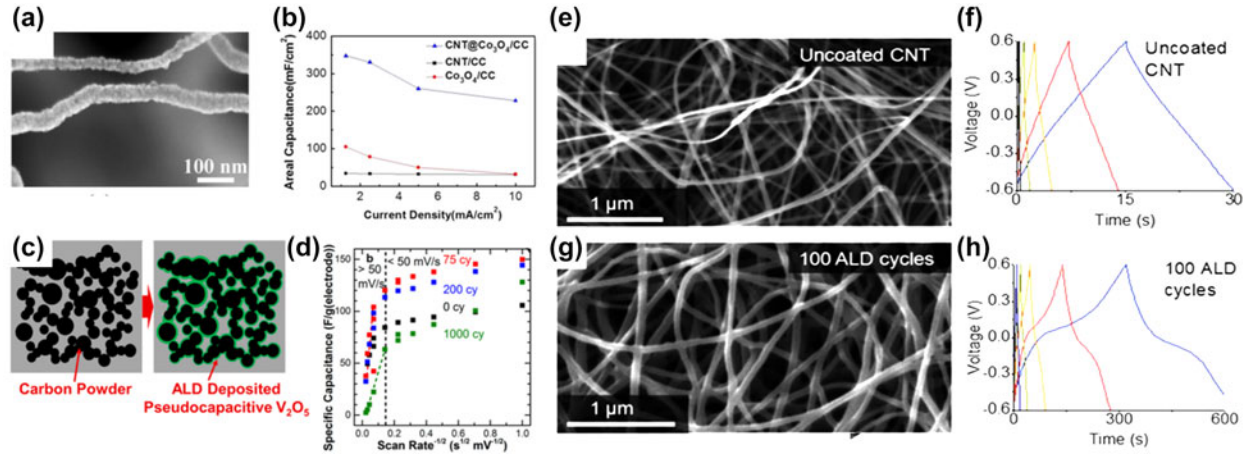


**Figure 6:** (a) The morphology and electrochemical performance of $Co_3O_4$ nanolayers on a flexible CC, (b) capacitance at various current densities of as-obtained composites. (a) and (b) are adapted from Ref. 127. (c) Schematic image of $V_2O_5$ thin films via ALD process on active carbon powders. (d) Specific capacitance at various scan rates, (c) and (d) are adapted from Ref. 128. (e) and (g) SEM images of uncoated CNT and smooth nanostructured vanadium oxide coatings on the surface of multiwalled carbon nanotube. (f) and (h) Charge discharge curves of as-obtained materials. (e)–(h) are adapted from Ref. 37.

extension, capture and limit the intermediate polysulfide inside the conductive matrix, and keep the ionic transfer interface stable, which led to the high performance of the Na–S batteries. Yu et al. [115] fabricated a graphene–sulfur composite with dual-protection by a compact graphene skin and ALD oxide coating for LSBs [see sample photos in Fig. 5(e)]. The enhanced performance can be ascribed to the preservation of the lithium polysulfide intermediates by the synergistic function of the graphene and the ALD-coated layer, which can enhance the structural stability.

## Applications of ALD in supercapacitors

Supercapacitors as a new-generation energy storage system hold excellent performance such as high power density, fast charge/discharge rate, and good cycling performance [1, 116, 117, 118, 119]. Supercapacitors are typically classified into electric double-layer capacitors (EDLCs) and pseudocapacitors. The mechanism of EDLCs can be attributed to electrostatic charge diffusion and accumulation at the interface of the electrode/electrolyte, whereas pseudocapacitors deliver high capacitance by Faradaic reactions at the electrode materials [120, 121, 122]. The pseudocapacitors could deliver more attractive values of energy density than EDLCs [123, 124, 125, 126].

Among various materials, transition metal oxides are viewed as an ideal electrode material for pseudocapacitors. Aimed to depositing active materials via ALD, Guan et al. [127] deposited $Co_3O_4$ nanolayers on a flexible carbon nanotubes/carbon cloth (CC) substrate by ALD [Fig. 6(a)]. The highest capacitances obtained for the CNT@2400–$Co_3O_4$/CC is 416.7 mF/cm$^2$ and the improvement can be attributed to the mechanically robust CC/CNTs substrate [Fig. 6(b)], the uniform coated high capacitance materials of $Co_3O_4$ nanoparticles, and the unique hierarchical structure. Parsons et al. [128] grew $V_2O_5$ thin films via ALD process on active carbon powders to form meso- and microporous carbon electrodes. As shown in Fig. 6(c), $V_2O_5$ ALD near the pore opening would block the pores, thus decreasing double layer capacitance. In addition, the $V_2O_5$ increased pseudocapacitance but decreased the accessible pores and double layer capacitance, leading to only a minimal change in overall capacitance at low ALD cycles. Also, the cyclic voltammetry scans for the ALD-coated carbon powders were less rectangular. A thicker $V_2O_5$ layer can increase total charge capacity, whereas a thinner $V_2O_5$ layer required shorter charge diffusion times, thus enabling quicker faradaic charge storage. Figure 6(d) demonstrates the great electrochemical performance in terms of large specific capacitance and good rate performance.

Boukhalfa et al. [37] designed a structure-allowed uniform deposition of smooth nanostructured vanadium oxide coatings on the surface of multiwalled carbon nanotube (CNT) electrodes, thus offering a novel route for the formation of binder-free flexible composite electrode fabric for supercapacitor applications

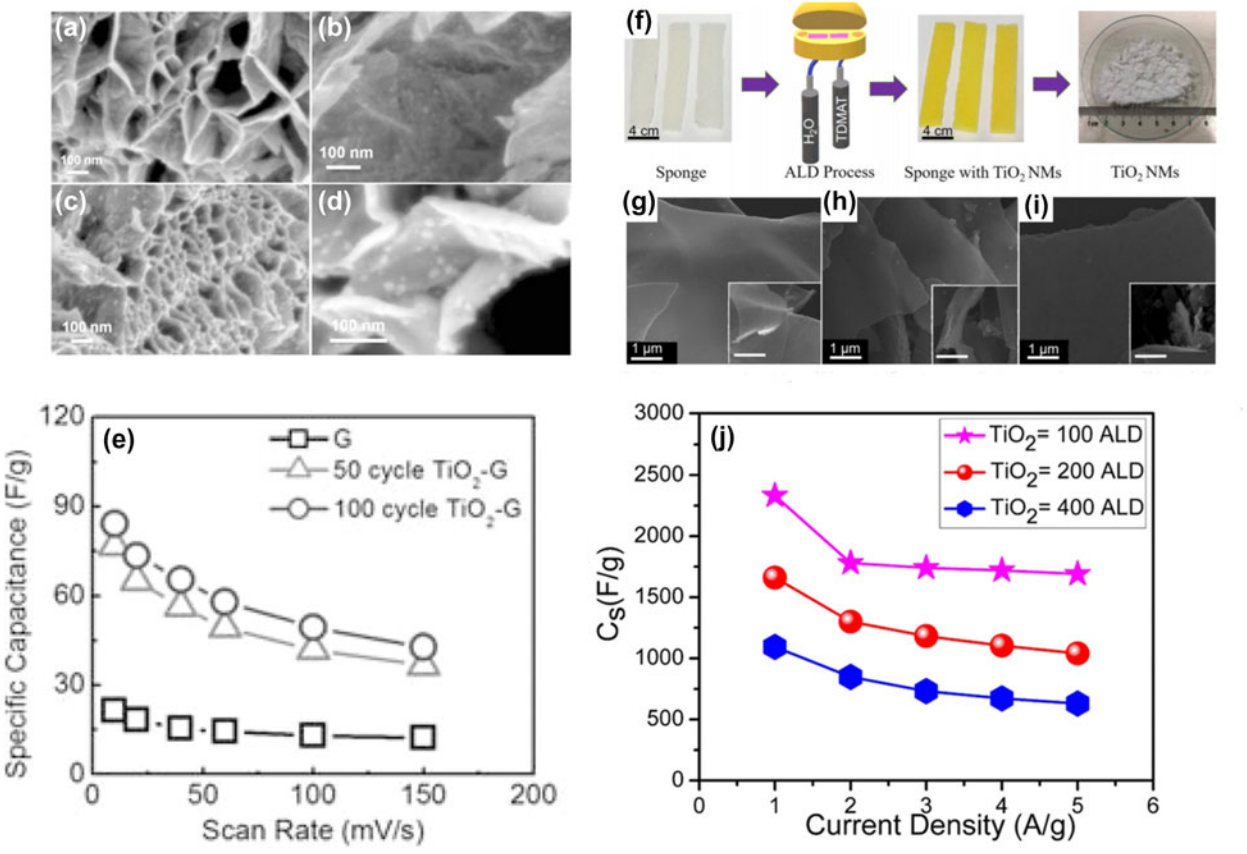


**Figure 7:** (a)–(d) SEM images of $TiO_2$–G composite grown different ALD cycles. (e) Specific capacitance at various scan rates. (a)–(e) are adapted from Ref. 35. (f)–(i) Fabrication process and morphologies of $TiO_2$ nanomembranes with different thicknesses. (f) Sketch represented fabrication process of $TiO_2$ nanomembranes. (g)–(i) SEM images of $TiO_2$ nanomembranes with 100, 200, and 400 ALD cycles, respectively. (j) Specific capacitance at various current densities. (f)–(j) are adapted from Ref. 80.

with greatly improved electrical conductivity and cycle stability [Figs. 6(e) and 6(g)]. As shown in Figs. 6(f) and 6(h), the electrochemical performance of capacitance largely enhanced by ALD vanadium oxide coating. With 100 ALD cycles, the composites exhibit pseudocapacitance.

Sun et al. [35] fabricated a nanoscaled coating of titanium oxide on graphene via a novel atomic ALD approach. The $TiO_2$ nanoparticles formed by ALD are homogeneously anchored onto the porous graphene sheets. The strong chemical bonding resulting from ALD ensures excellent electrical conductivity and stability throughout the entire three-dimensional network. In addition, $TiO_2$ provides pseudocapacitance and further enhanced the electrochemical performance. Figures 7(a)–7(d) show the SEM images of titanium oxide coatings on graphene, and Fig. 7(e) demonstrated the electrochemical performance in capacitance, which exhibits large capacitance and good rate capability. As a potential supercapacitor material, the composites exhibited a capacity of 75 F/g and 84 F/g at a scan rate of 10 mV/s for composites grown using 50 and 100 ALD cycles, respectively. The nearly identical Nyquist plots of the $TiO_2$–G composites compared with those of pure graphene demonstrated that the composites possess excellent conductivity for charge transfer and open structures for ion diffusion. Aimed to titanium oxide coatings through ALD technique, we recently fabricated $TiO_2$ nanomembranes with different thicknesses via ALD technique and used them for supercapacitor [Figs. 7(f)–7(i)] [80]. The uniform $TiO_2$ nanomembrane enhances the capacitance up to 2332 F/g at 1 A/g [Fig. 7(j)].

## Applications of ALD in biosensors

Sensors have important applications among society. They are widely applied to industrial emission monitor, biomedical, and agricultural related fields [129, 130, 131, 132]. Thanks to its excellent performance in thickness and composition control, as well as the conformallity; ALD can be applied in the preparation of various kinds of sensor devices [133, 134].

For directly depositing high catalytic active materials, Chio et al. [135] synthesized CNTs decorated with Ni by ALD [Fig. 8(a)]. The CNT-Ni composites exhibited high electrocatalytic activity for glucose oxidation in alkaline solutions. ALD can help Ni particles to be well deposited on CNTs, and this controllable construction led to an enhanced detection performance, such as high sensitivity, rapid response, wide linear response window, good selectivity, and repeatability for nonenzymatic detection. As shown in Fig. 8(b), CNT-Ni exhibits high sensitivity to target glucose and good selectivity. On the other hand, Yang et al. [78] used ALD to deposit NiO nanoparticles on SiC particles. The TEM images of composites were shown in Fig. 8(c). Taking advantages of ALD process, the NiO particles uniformly grew on SiC. As shown in Fig. 8(d), the NiO/SiC exhibits advantages of high glucose-sensing ability, low detection limit, high sensitivity, wide linear detection range, and good stability. The NiO/SiC prepared with 600 ALD cycles of NiO had the best sensing performance among the 200-, 400-, 600-, and 800-NiO/SiC with a sensitivity of 2.037 mA/(mM/cm$^2$). Zhang et al. [136] created a flexible electrode by depositing an ultrathin CoO layer on the skeleton surfaces of a nanoporous gold film by ALD [Fig. 8(e)]. The

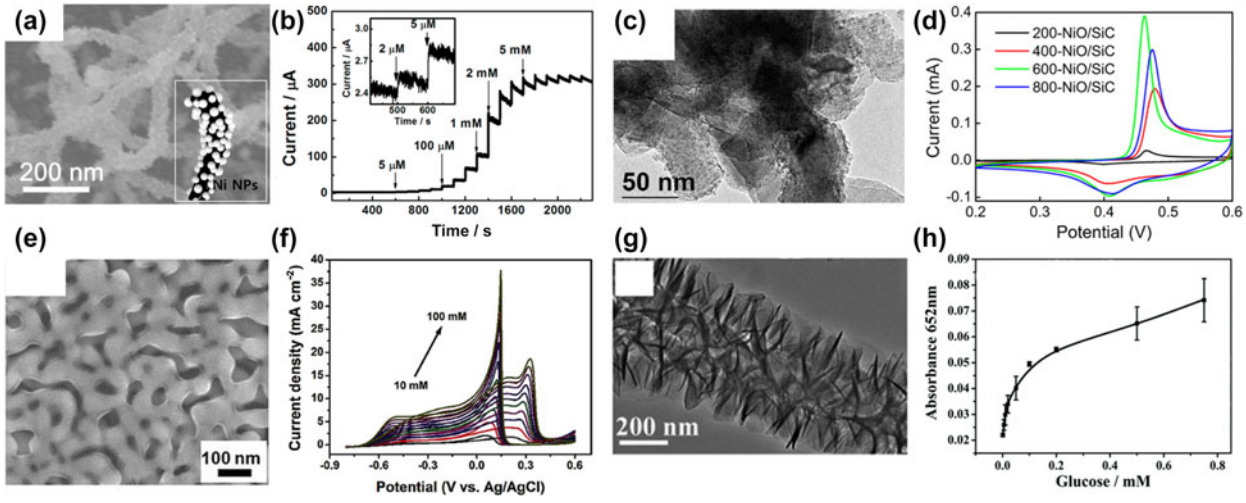


**Figure 8:** (a) SEM image of CNT–Ni composites. (b) Amperometric responses of the CNT–Ni–GCE with constant stirring in 0.1 M NaOH after successive glucose additions at $V_a$ of +0.50 V. Inset: the amperometric response to 2 and 5 μM. (a) and (b) are adapted from Ref. 135. (c) TEM images of NiO/SiC composites. (d) CV curves of NiO/SiC with different ALD cycles in 1 M KOH solution at a scan rate of 50 mV/s. (c) and (d) are adapted from Ref. 78. (e) SEM image of NPG films after CoO deposition with various ALD cycles. (f) CV curves of the NPG/CoO electrode in 0.5 m KOH solution with different amounts of glucose at a scan rate of 20 mV/s. (e) and (f) are adapted from Ref. 136. (g) TEM image of CF@CuAl-LDH. (h) Dose–response curve for glucose detection. (g) and (h) are adapted from Ref. 137.

https://doi.org/10.1557/jmr.2019.329 Published online by Cambridge University Press

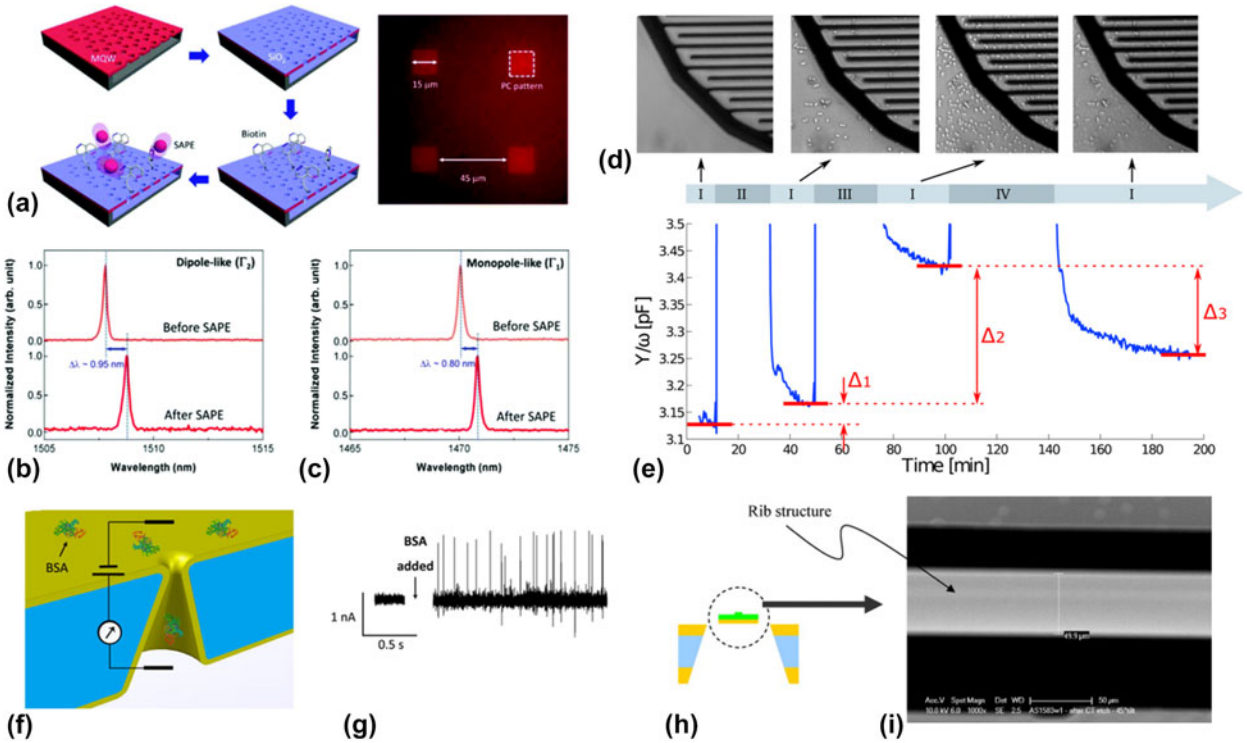


**Figure 9:** (a) Schematic surface functionalization steps for biosensing test. Graphs show the lasing spectra of the biosensors in (b) dipole-like Γ2 BEL mode and (c) monopole-like Γ1 BEL mode. Spectra in each plot are vertically shifted for clarity. (a)–(c) are adapted from Ref. 138. (d) and (e) The illustration of sensing events: (I) washing with PBS 1:1000, (II) incubating $5 \times 10^8$ CFU/mL *E. faecium* in synthetic urine, (III) incubating $5 \times 10^8$ CFU/mL *S. epidermidis* in synthetic urine and (IV) incubating lysostaphin. Shifts after wash $\Delta_1$, $\Delta_2$, and $\Delta_3$ are evaluated after the addition of *E. faecium*, *S. epidermidis*, and lytic enzymes, respectively. (d) and (e) are adapted from Ref. 82. (f) Schematic illustration of uniform ALD coating on a single conical nanochannel. (g) Example of current trace seen before and after adding buffered 100 nM BSA solution to the tip side of the conical nanochannel. (f) and (g) are adapted from Ref. 139. (h) and (i) The schematic image and SEM micrograph of a freestanding region of $TiO_2$ waveguide. (h) and (i) are adapted from Ref. 92.

hybrid showed high catalytic activity for glucose oxidation and $H_2O_2$ reduction due to the excellent synergistic performances of interfacial Au and CoO, as well as the gold skeleton with a large surface area. Because of high catalytic performance of the CoO layer, as shown in Fig. 8(f), the composites exhibit good sensitivity to target samples.

In addition, the ALD coatings as precursor and seed can take part in chemical reaction to form active materials. Recently, Wu et al. [137] used ALD to form uniform $Al_2O_3$ coating on carbon fiber to induce the growth of layered double hydroxide (LDH), and a carbon fiber-supported ultrathin CuAl LDH nanosheets (CF@CuAl-LDH) was obtained. The TEM image of CF@CuAl-LDH is shown in Fig. 8(g). In their work, $Al_2O_3$ was deposited by ALD at a deposition temperature of 150 °C. As shown in Fig. 8(h), the CF@CuAl-LDH had an excellent intrinsic peroxidase mimic activity for peroxidase substrate 3,3′,5,5′-tetramethylbenzidine (TMB), thus providing a rapid, sensitive, and selective colorimetric method for sensing glucose.

Because of good biocompatibility, ALD-prepared membrane can be used as transducer to load bioactive molecule. Utilizing this method, Tereshchenko et al. [84] reported their optical biosensor aimed for the determination of Grapevine virus A-type (GVA) proteins (GVA-antigens) based on ALD ZnO films. The GVA-antigen detection was performed by using the changes in the GVA-related light emission. The sensitivity of the biosensor was tested to be in the range from 1 pg/mL to 10 ng/mL of protein. Dominik et al. [85] deposited titanium oxide thin films on a long-period grating (LPG) induced in an optical fiber for the recognition of the complex formation between biotin and avidin. The sensitivity of the sensor was close to 3400 nm/RIU for LPG. Here, titanium oxide coating plays a role in modifying the sensor sensitivity, as well as enabling biofunctionalization and recovering process of the surface.

The uniform wrapping of thin films can provide great protection for whole device from harsh environment. Jeon et al. [138] reported a unique structure where $SiO_2$ films with a thickness of few nanometers were deposited on susceptible In–P wafer, which protected the underlying In–P from extremely harsh environments. Schematic surface functionalization steps for biosensing tests are shown in Fig. 9(a). Then, with the biotinylation of ALD-$SiO_2$ surface, chemical interaction between biotin and streptavidin molecules tagged with

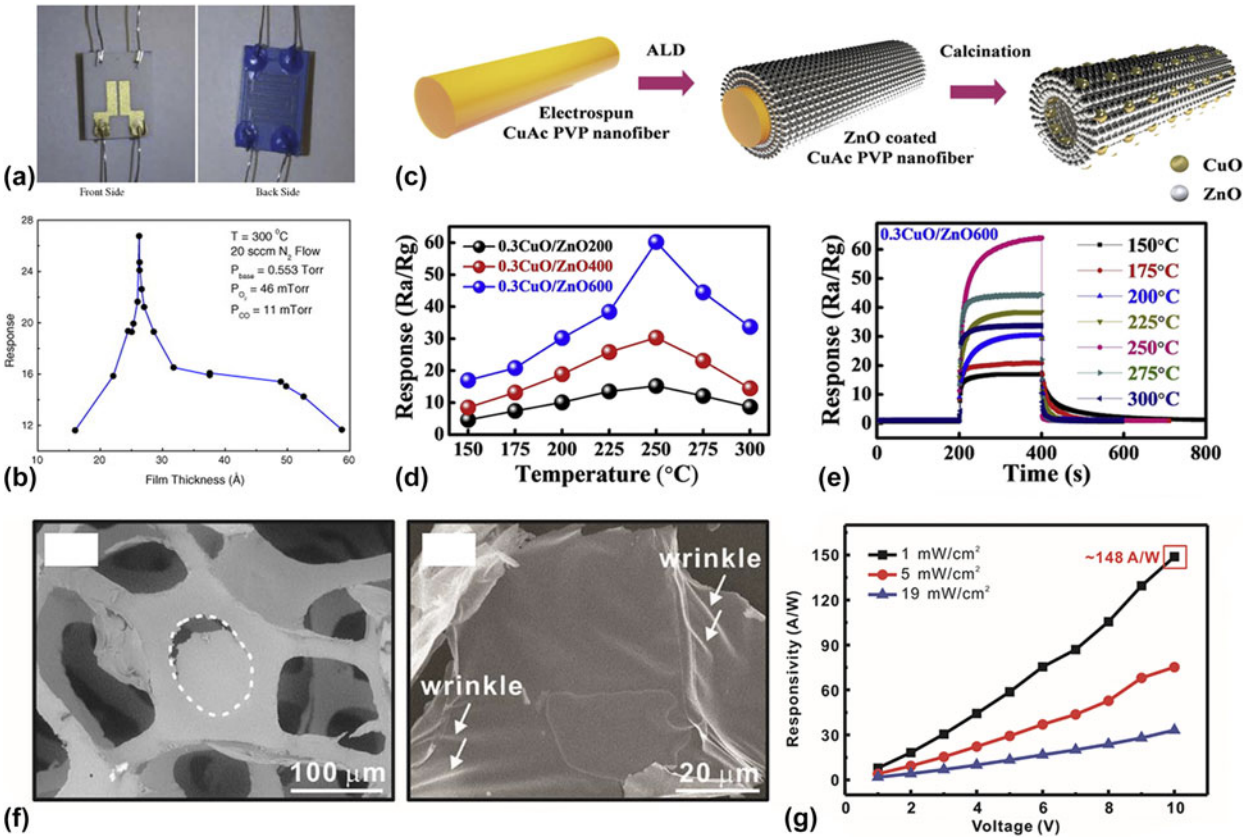


**Figure 10:** (a) Pictures of the front and back sides of the hotplate template. (b) Sensor response for a CO pressure of 11 m torr at 300 °C for different thicknesses of ALD $SnO_x$ films thicknesses. (a) and (b) are adapted from Ref. 142. (c) Schematic of 1D p-CuO/n-ZnO hollow nanofibers synthesis using a three-step method. (d) Responses of the 0.3 (g) CuO/ZnO200 (cycles), 0.3 (g) CuO/ZnO400 (cycles), and 0.3 (g) CuO/ZnO600 (cycles) HNFs sensors. (e) Dynamic resistance changes of 0.3CuO/ZnO600 HNFs sensor exposed to 100 ppm $H_2S$ as a function of operating temperature. (c)–(e) are adapted from Ref. 145. (f) SEM images of ZnO nanosheet on sponge and freestanding ZnO nanosheet. (g) Responsivity varying with the voltage under different irradiated power densities. (f)–(g) are adapted from Ref. 149.

phosphor (SAPE) allows the detection. As demonstrated in Figs. 9(b) and 9(c), the device decorated with ALD thin film is able to detect streptavidin with a large refractive index sensitivity of ~163 nm/RIU, and, meanwhile, generates a figure of merit of ~800. Flandre et al. [82] developed a novel structure for direct and selective detection of bacteria via lytic enzyme. The schematic for its function mechanism is demonstrated in Figs. 9(d) and 9(e). A CMOS-compatible chip was coated with a thin layer of ALD $Al_2O_3$ in average thickness of 30 nm. As the PDMS cap is pressed on the device, the whole microfluidic channel is formed [Fig. 9(d)]. The incubation of lytic enzyme was able to function with target bacteria in the matrix flow, thus accomplish the whole bacteria detection. The $Al_2O_3$ layer protected the chip from corrosion of electrolyte and reduced the detrimental effects on bacterial sensitivity. As shown in Fig. 9(e), because of the protection of ALD $Al_2O_3$, the sensors exhibited an outstanding detection limit of approximately $10^8$ (CFU/mL) min in a 1.5 μL microfluidic chamber with an additional setup time of 50 min.

Because of the stability of films based on ALD, the protective shell made from ALD technique broadens the application in regenerated biosensors. Xue et al. [139] designed a conical nanochannel for protein sensing. The unique structure was built by track-etching and then modified via ALD $Al_2O_3$. With the conformal depositing, $Al_2O_3$ thin film coated on the surface uniformly and constructed resultant nanochannels [Fig. 9(f)]. The conical nanochannels can hinder the travel rate of bovine serum albumin to enhance the capture rate with excellent signal-to-noise ratio for the transport events [Fig. 9(g)]. Purniawan et al. [140] developed a freestanding structure of rib via ALD-deposited $TiO_2$ [Figs. 9(h) and 9(i)], which was selective to Escherichia coli, and used the structure to sense its presence. The sensitivity, evaluated by evaporation of several concentrations of ethanol and isopropyl alcohol diluted in water, was found to be 0.85 and 1.34 dB/% (v/v), respectively.

It is worth noting that some nanoarchitectures fabricated by ALD have similar dimensions with the biological components of the biorecognition film, and therefore draw considerable attention. Comstock et al. [141] produced rough Pt films via template-assisted ALD coating, as characterized by roughness factors as large as 310. The nanostructured Pt film was

https://doi.org/10.1557/jmr.2019.329 Published online by Cambridge University Press

applied in enzyme-free glucose sensing and displayed a desirable near-linear response to glucose in the range of 0–20 m M with a sensitivity of 63.8 μA/(cm$^2$/mM).

## Applications of ALD in other sensors

Gas sensors are widely used in industrial emission monitor and environment protection field. ALD technique has also been extensively applied. Du et al. [142] prepared ultrathin $SnO_x$ films by ALD and the $SnO_x$ films can be served as a CO gas sensor, of which maximum response for CO gas sensing was observed at a $SnO_x$ film with a thickness of 26.2 Å. The pictures of the front and back sides of the hotplate template are shown in Fig. 10(a). The response of gas sensor was temperature dependent and displayed its highest responsivity at temperatures between 250 and 325 °C. Sensor response for a CO pressure of 11 m torr at 300 °C for different $SnO_x$ ALD film thicknesses grown on separate hotplate templates is shown in Fig. 10(b). Niskanen et al. [143] used ALD to produce gas-sensitive tin dioxide film in a microhotplate gas sensor. Ethanol, acetone, and acrylonitrile were used as model analytes to investigate the device performance. The results demonstrated good response, low drift rates of the output signal, and good operational stability in the short term.

Yun et al. [144] reported $NH_3$ gas sensors with semiconductor thin-film transistor (TFT) configuration using ALD ZnO nanoparticles as gas-sensing element. Oxygen molecules on the surface of exposed sensing materials in atmosphere extract the electrons from the conduction band in ZnO nanoparticles to form oxygen ions when thermal energy is supplied, and when contacted with $NH_3$ gas, by-products such as $NH_4OH$ were generated and the conductivity changes can be observed by measuring drain current ($I_{DS}$) of TFT. The device showed high sensitivity to target gas, excellent retrievability after the gas removal, and stable device performance even after the repeated measurements.

On the other hand, Han et al. [145] reported the fabrication of 1D p-CuO/n-ZnO hollow nanofibers with high detection performance for $H_2S$ by the combination of electrospinning and ALD technique [Fig. 10(c)]. Taking advantages of ALD, the ratios of Zn to Cu ($R_{Zn/Cu}$) was controlled, which optimized the repeated gas-sensing performance. The optimum response of these materials was improved about 6-fold versus the neat ZnO and 45-fold versus neat CuO. Meanwhile, an improvement in the selectivity and stability of these $H_2S$ sensors was also observed [Figs. 10(d) and 10(e)].

In addition, ALD can also take part in the fabrication of pH sensors. Lin et al. [146] reported an light-immune pH sensor with a SiC-based electrolyte-insulator-semiconductor structure, which overcame the problem caused by light penetration. 10 nm ALD $HfO_2$ was deposited on the supporting wafer. This device reached an average pH sensitivity of 52.35 mV/pH and had a low light response (3.9–8.6 mV) due to its intrinsic property of having a wide band gap. Jakob et al. [147] used low-temperature ALD to fabricate ZnO and $Al_2O_3$ thin films for pH sensor. The $Al_2O_3$ thin film was applied as a sensitive layer on the ZnO thin film, and meanwhile acted as a gate oxide between the liquid gate potential and the ZnO channel. This small volume potentiometric pH sensor based on flexible and transparent field effect transistors had a good pH sensitivity for wide pH ranging from 5 to 10. Recently, Wang et al. [148] enhanced the pH sensitivity of AlGaN/GaN ion-sensitive field-effect transistor (ISFET) by coating an ALD $Al_2O_3$ layer on its sensing area. The $Al_2O_3$ coating not only successfully reduced the surface state density and the current in the solution but also induced higher density of sensing site as well as better surface hydrophilicity, leading to an improved sensitivity of 57.8 mV/pH for the $Al_2O_3$-ISFET. Recently, Guo et al. [149] developed a simple and convenient approach to synthesize large amounts of ZnO nanosheets [Fig. 10(f)], which are suitable for producing the key component of printed ultraviolet photodetectors. As shown in Fig. 10(g), the obtained printed ultraviolet photodetector that utilizes ZnO nanosheets as the functional materials exhibits a high responsivity of ~148 A/W and a response time of 19 s.

## Summary and outlook

In the past decade, ALD has undergone tremendous progress and become an efficient technique for nanostructures fabrication. In many studies, ALD was proven to be valuable because of its ability to improve device performance. Thanks to its ability to fabricate advanced nanostructures and generate uniform coatings on the surface, ALD has become one of the most promising deposition methods and is used in a variety of applications.

The films deposited by ALD are of extremely high quality and precise thickness and composition control, while also providing a high degree of uniformity, which is a significant capability in the fabrication of novel nanostructures. Therefore, ALD is widely used for active material growth and deposition, formation of protective layers, and direct establishment of nanostructures. These aspects are well represented in applications like supercapacitors, batteries, and sensors. For batteries, ALD can be applied to structure engineering/modification layer formation for better performance. The active electrode materials for excellent electrochemical performance and controllable physical properties, as well as passivation layer to get electrodes free from the threats from the working environment, were fabricated and investigated. In addition, good biocompatibility makes ALD work well in biosensors and can be used for the sensing of glucose (both enzyme detection and enzyme-free

https://doi.org/10.1557/jmr.2019.329 Published online by Cambridge University Press

detection), protein, etc. Other types of sensors are also becoming more sensitive because of ALD, including but not limited to some gas sensors and pH sensors.

However, there is still a long way to go before ALD comes to scale application. ALD now remains a relatively slow method than other conventional deposition methods. To solve this problem, many enhancements, e.g., plasma, which can lower the reaction temperature and accelerate the reaction rate, have been induced to the system. Based on the advantages of ALD technology itself and existing researches, we can say with certainty that ALD will still be in a rapid development stage. We believe it will be more commonly used in energy storage applications and sensor devices as well as many other fields. With the increasing emphasis on this field and the development of ALD technology itself, the large-scale application of ALD-based nanostructures will make this technology more affordable in the future.

## Acknowledgments

This work was supported by the Natural Science Foundation of China (Nos. 61975035 and U1632115), Science and Technology Commission of Shanghai Municipality (No. 17JC1401700), the National Key R&D Program of China (Nos. 2017YFE0112000 and 2015ZX02102-003), and the Program of Shanghai Academic Research Leader (19XD1400600).

## References

1. **Z. Zhao, S.L. Liu, J.X. Zhu, J.S. Xu, L. Li, Z.Q. Huang, C. Zhang, and T.X. Liu**: Hierarchical nanostructures of nitrogen-doped porous carbon polyhedrons confined in carbon nanosheets for high-performance supercapacitors. *ACS Appl. Mater. Interfaces* **10**, 19871 (2018).
2. **B.Y. Lee, D.H. Kim, J. Park, K-I. Park, K.J. Lee, and C.K. Jeong**: Modulation of surface physics and chemistry in triboelectric energy harvesting technologies. *Sci. Technol. Adv. Mater.* **20**, 758 (2019).
3. **G.S. Huang and Y.F. Mei**: Assembly and self-assembly of nanomembrane materials-from 2D to 3D. *Small* **14**, 1703665 (2018).
4. **M. Liu, B. Liu, Q.Q. Liu, K.K. Du, Z.F. Wang, and N.Y. He**: Nanomaterial-induced ferroptosis for cancer specific therapy. *Coord. Chem. Rev.* **382**, 160 (2019).
5. **H.Y. Jin, C.X. Guo, X. Liu, J.L. Liu, A. Vasileff, Y. Jiao, Y. Zheng, and S.Z. Qiao**: Emerging two-dimensional nanomaterials for electrocatalysis. *Chem. Rev.* **118**, 6337 (2018).
6. **M. Huang, F. Cavallo, F. Liu, and M.G. Lagally**: Nanomechanical architecture of semiconductor nanomembranes. *Nanoscale* **3**, 96 (2011).
7. **M.B. Zheng, H. Tang, L.L. Li, Q. Hu, L. Zhang, H.G. Xue, and H. Pang**: Hierarchically nanostructured transition metal oxides for lithium-ion batteries. *Adv. Sci.* **5**, 1700592 (2018).
8. **B. Fang, J.H. Kim, M.S. Kim, and J.S. Yu**: Hierarchical nanostructured carbons with meso-macroporosity: Design, characterization, and applications. *Acc. Chem. Res.* **46**, 1397 (2013).
9. **S. Ding, D. Zhang, J.S. Chen, and X.W. Lou**: Facile synthesis of hierarchical $MoS_2$ microspheres composed of few-layered nanosheets and their lithium storage properties. *Nanoscale* **4**, 95 (2012).
10. **M. Radovic, G. Dubourg, Z. Dohcevic-Mitrovic, B. Stojadinovic, J. Vukmirovic, N. Samardzic, and M. Bokorov**: $SnO_2$ nanosheets with multifunctional properties for flexible gas-sensors and UVA light detectors. *J. Phys. D Appl. Phys.* **52**, 385305 (2019).
11. **S. Janghela, S. Devi, N. Kambo, D. Roy, K. Mukhopadhyay, and N.E. Prasad**: Microphase separation in oriented polymeric chains at the surface of nanomaterials during nanofiber formation. *Soft Matter* **15**, 6811 (2019).
12. **Y. Cheng, Y. Chang, Y.L. Feng, H. Jian, X.Q. Wu, R.X. Zheng, L. Wang, X.M. Ma, K.Q. Xu, P.P. Song, Y.J. Wang, and H.Y. Zhang**: Hierarchical acceleration of wound healing through intelligent nanosystem to promote multiple stages. *ACS Appl. Mater. Interfaces* **11**, 33725 (2019).
13. **B.M. Abu-Zied and K.A. Alamry**: Green synthesis of 3D hierarchical nanostructured $Co_3O_4$/carbon catalysts for the application in sodium borohydride hydrolysis. *J. Alloys Compd.* **798**, 820 (2019).
14. **W.T. Zhu, H.H. Chen, J.W. Yang, W.X. Cai, Z.Q. Bao, and X.F. Zhou**: One-pot fabrication of $TiO_2$ rutile nanorods/anatase nanoparticles: Mixed crystal phase and morphology-control for enhanced photovoltaic performance. *J. Nanosci. Nanotechnol.* **19**, 7714 (2019).
15. **M.A. Pimenta, G. Dresselhaus, M.S. Dresselhaus, L.G. Cancado, A. Jorio, and R. Saito**: Studying disorder in graphite-based systems by Raman spectroscopy. *Phys. Chem. Chem. Phys.* **9**, 1276 (2007).
16. **P. Dai, Y. Jiao, H.L. Ma, X.M. Zeng, Y.J. Lu, L.C. Wang, M. Bao, and M.L. Zhai**: Radiation synthesis of polysilane-modified graphene oxide for improving thermal conductivity and mechanical properties of silicone rubber. *J. Appl. Polym. Sci.* **136**, 47776 (2019).
17. **S. Linic, P. Christopher, and D.B. Ingram**: Plasmonic-metal nanostructures for efficient conversion of solar to chemical energy. *Nat. Mater.* **10**, 911 (2011).
18. **D. Li, M.B. Mueller, S. Gilje, R.B. Kaner, and G.G. Wallace**: Processable aqueous dispersions of graphene nanosheets. *Nat. Nanotechnol.* **3**, 101 (2008).
19. **P.O. Oviroh, R. Akbarzadeh, D. Pan, R.A.M. Coetzee, and T.C. Jen**: New development of atomic layer deposition: Processes,

methods and applications. *Sci. Technol. Adv. Mater.* **20**, 465 (2019).

20. **A. Sutka, M. Jarvekulg, and K.A. Gross**: Photocatalytic nanoheterostructures and chemically bonded junctions made by solution-based approaches. *Crit. Rev. Solid State Mater. Sci.* **44**, 239 (2019).
21. **Y. Zhang, Y. Yang, H. Sun, and J. Wang**: Synthesis of $TiB_2$ powders with hexagonal morphology by sol–gel method. *J. Nanosci. Nanotechnol.* **19**, 7886 (2019).
22. **R. Yang, Z. Gong, X. Zhang, and L. Que**: Single-walled carbon nanotubes (SWCNTs) and poly(3,4-ethylenedioxythiophene) nanocomposite microwire-based electronic biosensor fabricated by microlithography and layer-by-layer nanoassembly. *J. Nanosci. Nanotechnol.* **19**, 7591 (2019).
23. **M. Nazari, S. Kashanian, and R. Mohammadi**: Electrodeposition of anionic, cationic and nonionic surfactants and gold nanoparticles onto glassy carbon electrode for catechol detection. *J. Nanoanalysis* **6**, 48 (2019).
24. **O.M. Dawood, R.K. Gupta, U. Monteverde, F.H. Alqahtani, H-Y. Kim, J. Sexton, R.J. Young, M. Missous, and M.A. Migliorato**: Dynamic modulation of the Fermi energy in suspended graphene backgated devices. *Sci. Technol. Adv. Mater.* **20**, 568 (2019).
25. **M.C. Tseng, D.S. Wuu, C.L. Chen, H.Y. Lee, C.Y. Chien, P.L. Liu, and R.H. Horng**: Characteristics of atomic layer deposition-grown zinc oxide thin film with and without aluminum. *Appl. Surf. Sci.* **491**, 535 (2019).
26. **S. Lee, Y. Lee, J. Park, W. Yu, G.Y. Cho, Y. Kim, and S.W. Cha**: Effect of plasma-enhanced atomic layer deposited YSZ inter-layer on cathode interface of GDC electrolyte in thin film solid oxide fuel cells. *Renew. Energ.* **144**, 123 (2019).
27. **Y. Kim, M. Chang, S. Cho, M. Kim, H. Kim, E. Choi, H. Ko, J. Hwang, and B. Park**: Formation of a functional homo-junction interface through ZnO atomic layer passivation: Enhancement of carrier mobility and threshold voltage in a ZnO nanocrystal field effect transistor. *J. Alloy. Compd.* **804**, 213 (2019).
28. **S. Zhu, J. Liu, and J. Sun**: Precise growth of $Al_2O_3/SnO_2$/CNTs composites by a two-step atomic layer deposition and their application as an improved anode for lithium ion batteries. *Electrochim. Acta* **319**, 490 (2019).
29. **R. Solanki, J. Huo, J.L. Freeouf, and B. Miner**: Atomic layer deposition of ZnSe/CdSe superlattice nanowires. *Appl. Phy. Lett.* **81**, 3864 (2002).
30. **B. Ahmed, C. Xia, and H.N. Alshareef**: Electrode surface engineering by atomic layer deposition: A promising pathway toward better energy storage. *Nano Today* **11**, 250 (2016).
31. **D. Chen, Z. Kang, H. Hirahara, S. Aisawa, and W. Li**: Adsorption behaviors of deposition-targeted metallic ions onto thiol-containing silane modified liquid crystal polymer surfaces. *Appl. Surf. Sci.* **479**, 368 (2019).
32. **M. Knez, A. Kadri, C. Wege, U. Gosele, H. Jeske, and K. Nielsch**: Atomic layer deposition on biological macromolecules: Metal oxide coating of tobacco mosaic virus and ferritin. *Nano Lett.* **6**, 1172 (2006).
33. **X. Li, X. Meng, J. Liu, D. Geng, Y. Zhang, M.N. Banis, Y. Li, J. Yang, R. Li, X. Sun, M. Cai, and M.W. Verbrugge**: Tin oxide with controlled morphology and crystallinity by atomic layer deposition onto graphene nanosheets for enhanced lithium storage. *Adv. Funct. Mater.* **22**, 1647 (2012).
34. **Y.S. Jung, A.S. Cavanagh, L.A. Riley, S.H. Kang, A.C. Dillon, M.D. Groner, S.M. George, and S.H. Lee**: Ultrathin direct atomic layer deposition on composite electrodes for highly durable and safe Li-ion batteries. *Adv. Mater.* **22**, 2172 (2010).
35. **X. Sun, M. Xie, G. Wang, H. Sun, A.S. Cavanagh, J.J. Travis, S.M. George, and J. Lian**: Atomic layer deposition of $TiO_2$ on graphene for supercapacitors. *J. Electrochem. Soc.* **159**, A364 (2012).
36. **C. Guan, X. Xia, N. Meng, Z. Zeng, X. Cao, C. Soci, H. Zhang, and H.J. Fan**: Hollow core–shell nanostructure supercapacitor electrodes: Gap matters. *Energy Environ. Sci.* **5**, 9085 (2012).
37. **S. Boukhalfa, K. Evanoff, and G. Yushin**: Atomic layer deposition of vanadium oxide on carbon nanotubes for high-power supercapacitor electrodes. *Energy Environ. Sci.* **5**, 6872 (2012).
38. **A.M. van der Zande, P.Y. Huang, D.A. Chenet, T.C. Berkelbach, Y. You, G.H. Lee, T.F. Heinz, D.R. Reichman, D.A. Muller, and J.C. Hone**: Grains and grain boundaries in highly crystalline monolayer molybdenum disulphide. *Nat. Mater.* **12**, 554 (2013).
39. **S. Hofmann, R. Sharma, C. Ducati, G. Du, C. Mattevi, C. Cepek, M. Cantoro, S. Pisana, A. Parvez, F. Cervantes-Sodi, A.C. Ferrari, R. Dunin-Borkowski, S. Lizzit, L. Petaccia, A. Goldoni, and J. Robertson**: In situ observations of catalyst dynamics during surface-bound carbon nanotube nucleation. *Nano Lett.* **7**, 602 (2007).
40. **Z. Zhao, Z.W. Zhang, Y.T. Zhao, J.R. Liu, C. Liu, Z.J. Wang, G.F. Zheng, G.S. Huang, and Y.F. Mei**: Atomic layer deposition inducing integration of Co, N codoped carbon sphere on 3D foam with hierarchically porous structures for flexible hydrogen producing device. *Adv. Funct. Mater.* 1906365 (2019).
41. **S. Ratan, C. Kumar, A. Kumar, D.K. Jarwal, A.K. Mishra, R.K. Upadhyay, and S. Jit**: Fabrication and characterization of a ZnO quantum dots-based metal-semiconductor-metal sensor for hydrogen gas. *Nanotechnology* **30**, 395501 (2019).
42. **M.L. Huang, Y.C. Chang, C.H. Chang, Y.J. Lee, P. Chang, J. Kwo, T.B. Wu, and M. Hong**: Surface passivation of III–V compound semiconductors using atomic-layer-deposition-grown $Al_2O_3$. *Appl. Phy. Lett.* **87**, 252104 (2005).
43. **H.C.M. Knoops, M.E. Donders, L. Baggetto, M. Sanden, P.H.L. Notten, and W.M.M. Kessels**: Atomic layer deposition for all-solid-state 3D-integrated batteries. *ECS Trans.* **25**, 333 (2009).

44. **M. Reghima, A. Akkari, C. Guasch, and N. Kamoun-Turki**: Effect of indium doping on physical properties of nanocrystallized SnS zinc blend thin films grown by chemical bath deposition. *J. Renew. Sustain. Ener.* **4**, 011602 (2012).
45. **T.B. Nasr, N. Kamoun, and C. Guasch**: Physical properties of ZnS thin films prepared by chemical bath deposition. *Appl. Surf. Sci.* **254**, 5039 (2008).
46. **K. Baek, C. Jin, J. Lee, B.Y. Jeong, W.I. Lee, and C. Lee**: Structure and photoluminescence properties of ZnS nanowires sheathed with $SnO_2$ by atomic layer deposition. *J. Mater. Sci.* **45**, 3851 (2010).
47. **S.M. George**: Atomic layer deposition: An overview. *Chem. Rev.* **110**, 111 (2010).
48. **R.L. Puurunen**: Surface chemistry of atomic layer deposition: A case study for the trimethylaluminum/water process. *J. Appl. Phy.* **97**, 121301 (2005).
49. **M.D. Groner, F.H. Fabreguette, J.W. Elam, and S.M. George**: Low-temperature $Al_2O_3$ atomic layer deposition. *Chem. Mater.* **16**, 639 (2004).
50. **J.S. Wellings, N.B. Chaure, S.N. Heavens, and I.M. Dhannadasa**: Growth and characterisation of electrodeposited ZnO thin films. *Thin Solid Films* **516**, 3893 (2008).
51. **M. Schreier, F. Heroguel, L. Steier, S. Ahmad, J.S. Luterbacher, M.T. Mayer, J. Luo, and M. Gratzel**: Solar conversion of $CO_2$ to CO using earth-abundant electrocatalysts prepared by atomic layer modification of CuO. *Nat. Energy* **2**, 17087 (2017).
52. **L. Niinisto, J. Paivasaari, J. Niinisto, M. Putkonen, and M. Nieminen**: Advanced electronic and optoelectronic materials by atomic layer deposition: An overview with special emphasis on recent progress in processing of high-*k* dielectrics and other oxide materials. *Phys. Status Solidi a* **201**, 1443 (2004).
53. **C. Guan, X. Wang, Q. Zhang, Z. Fan, H. Zhang, and H.J. Fan**: Highly stable and reversible lithium storage in $SnO_2$ nanowires surface coated with a uniform hollow shell by atomic layer deposition. *Nano Lett.* **14**, 4852 (2014).
54. **H. Zhao, H. Gao, B. Li, Z. Song, T. Hu, and F. Liu**: Atomic layer deposition of $V_2O_5$ on nitrogen-doped graphene as an anode for lithium-ion batteries. *Mater. Lett.* **252**, 215 (2019).
55. **Z. Szabo, J. Volk, Z.E. Horvath, Z. Medveczky, Z. Czigany, K. Vad, and Z. Baji**: Atomic layer deposition and annealing of Ga doped ZnO films. *Mater. Sci. Semi. Process.* **101**, 95 (2019).
56. **T. Tynell and M. Karppinen**: Atomic layer deposition of ZnO: A review. *Semicond. Sci. Technol.* **29**, 043001 (2014).
57. **A.C. Kozen, C.F. Lin, A.J. Pearse, M.A. Schroeder, X.G. Han, L.B. Hu, S.B. Lee, G.W. Rubloff, and M. Noked**: Next-generation lithium metal anode engineering via atomic layer deposition. *ACS Nano* **9**, 5884 (2015).
58. **J. Robertson**: High dielectric constant gate oxides for metal oxide Si transistors. *Rep. Prog. Phys.* **69**, 327 (2006).
59. **C. Park, J. Yoon, and E.L. Thomas**: Enabling nanotechnology with self assembled block copolymer patterns. *Polymer* **44**, 6725 (2003).
60. **D. Golberg, Y. Bando, Y. Huang, T. Terao, M. Mitome, C. Tang, and C. Zhi**: Boron nitride nanotubes and nanosheets. *ACS Nano* **4**, 2979 (2010).
61. **J.S. King, D. Heineman, E. Graugnard, and C.J. Summers**: Atomic layer deposition in porous structures: 3D photonic crystals. *Appl. Surf. Sci.* **244**, 511 (2005).
62. **Y.J. Kwack and W.S. Choi**: Chemical vapor deposition-free solution-processed synthesis method for two-dimensional $MoS_2$ atomic layer films. *Nanotechnology* **30**, 38 (2019).
63. **M. Leskela and M. Ritala**: Atomic layer deposition (ALD): From precursors to thin film structures. *Thin Solid Films* **409**, 138 (2002).
64. **E. Kim, Y. Vaynzof, A. Sepe, S. Guldin, M. Scherer, P. Cunha, S.V. Roth, and U. Steiner**: Gyroid-structured 3D ZnO networks made by atomic layer deposition. *Adv. Funct. Mater.* **24**, 863 (2014).
65. **K.E. Gregorczyk, A.C. Kozen, X. Chen, M.A. Schroeder, M. Noked, A. Cao, L. Hu, and G.W. Rubloff**: Fabrication of 3D core–shell multiwalled carbon nanotube@$RuO_2$ lithium-ion battery electrodes through a $RuO_2$ atomic layer deposition process. *ACS Nano* **9**, 464 (2015).
66. **C. Bae, H. Shin, and K. Nielsch**: Surface modification and fabrication of 3D nanostructures by atomic layer deposition. *MRS Bull.* **36**, 887 (2011).
67. **X. Zhang, J. Zhao, A.V. Whitney, J.W. Elam, and R.P. Van Duyne**: Ultrastable substrates for surface-enhanced Raman spectroscopy: $Al_2O_3$ overlayers fabricated by atomic layer deposition yield improved anthrax biomarker detection. *J. Am. Chem. Soc.* **128**, 10304 (2006).
68. **M. Ritala, K. Kukli, A. Rahtu, P.I. Raisanen, M. Leskela, T. Sajavaara, and J. Keinonen**: Atomic layer deposition of oxide thin films with metal alkoxides as oxygen sources. *Science* **288**, 319 (2000).
69. **E. Bonera, G. Scarel, and M. Fanciulli**: Structure evolution of atomic layer deposition grown $ZrO_2$ films by deep-ultra-violet Raman and far-infrared spectroscopies. *J. Non-Cryst. Solids* **322**, 105 (2003).
70. **J. Johansson, J. Kostamo, M. Karppinen, and L. Niinisto**: Growth of conductive copper sulfide thin films by atomic layer deposition. *J. Mater. Chem.* **12**, 1022 (2002).
71. **Q. Zhang, C.S. Dandeneau, X. Zhou, and G. Cao**: ZnO nanostructures for dye-sensitized solar cells. *Adv. Mater.* **21**, 4087 (2009).
72. **X. Yang, A. Wolcott, G. Wang, A. Sobo, R.C. Fitzmorris, F. Qian, J.Z. Zhang, and Y. Li**: Nitrogen-doped ZnO nanowire arrays for photoelectrochemical water splitting. *Nano Lett.* **9**, 2331 (2009).
73. **V. Miikkulainen, M. Leskela, M. Ritala, and R.L. Puurunen**: Crystallinity of inorganic films grown by atomic layer deposition: Overview and general trends. *J. Appl. Phys.* **113**, 021301 (2013).

74. **Z. Yin, S. Wu, X. Zhou, X. Huang, Q. Zhang, F. Boey, and H. Zhang**: Electrochemical deposition of ZnO nanorods on transparent reduced graphene oxide electrodes for hybrid solar cells. *Small* **6**, 307 (2010).
75. **B.J. Choi, D.S. Jeong, S.K. Kim, C. Rohde, S. Choi, J.H. Oh, H.J. Kim, C.S. Hwang, K. Szot, R. Waser, B. Reichenberg, and S. Tiedke**: Resistive switching mechanism of $TiO_2$ thin films grown by atomic-layer deposition. *J. Appl. Phy.* **98**, 033715 (2005).
76. **J.S. Daubert, J.Z. Mundy, and G.N. Parsons**: Kevlar-based supercapacitor fibers with conformal pseudocapacitive metal oxide and metal formed by ALD. *Adv. Mater. Interfaces* **3**, 1600355 (2016).
77. **P. Banerjee, W-J. Lee, K-R. Bae, S.B. Lee, and G.W. Rubloff**: Structural, electrical, and optical properties of atomic layer deposition Al-doped ZnO films. *J. Appl. Phy.* **108**, 043504 (2010).
78. **P. Yang, X. Tong, G. Wang, Z. Gao, X. Guo, and Y. Qin**: NiO/SiC nanocomposite prepared by atomic layer deposition used as a novel electrocatalyst for nonenzymatic glucose sensing. *ACS Appl. Mater. Interfaces* **7**, 4772 (2015).
79. **Y.T. Zhao, G.S. Huang, D.R. Wang, Y. Ma, Z. Fan, Z. Bao, and Y.F. Mei**: Sandwiched porous C/ZnO/porous C nanosheet battery anodes with a stable solid-electrolyte interphase for fast and long cycling. *J. Mater. Chem. A* **6**, 22870 (2018).
80. **F. Naeem, S. Naeem, Y.T. Zhao, D.R. Wang, J. Zhang, Y.F. Mei, and G.S. Huang**: $TiO_2$ nanomembranes fabricated by atomic layer deposition for supercapacitor electrode with enhanced capacitance. *Nanoscale Res. Lett.* **14**, 92 (2019).
81. **M. Schindler, S.K. Kim, C.S. Hwang, C. Schindler, A. Offenhaeusser, and S. Ingebrandt**: Novel post-process for the passivation of a CMOS biosensor. *Phys. Status. Solidi Rapid Res. Lett.* **2**, 4 (2008).
82. **N. Couniot, T. Vanzieleghem, J. Rasson, N. Van Overstraeten-Schloegel, O. Poncelet, J. Mahillon, L.A. Francis, and D. Flandre**: Lytic enzymes as selectivity means for label-free, microfluidic and impedimetric detection of whole-cell bacteria using ALD-$Al_2O_3$ passivated microelectrodes. *Biosens. Bioelectron.* **67**, 154 (2015).
83. **H. Im, N.C. Lindquist, A. Lesuffleur, and S-H. Oh**: Atomic layer deposition of dielectric overlayers for enhancing the optical properties and chemical stability of plasmonic nanoholes. *ACS Nano* **4**, 947 (2010).
84. **A. Tereshchenko, V. Fedorenko, V. Smyntyna, I. Konup, A. Konup, M. Eriksson, R. Yakimova, A. Ramanavicius, S. Balme, and M. Bechelany**: ZnO films formed by atomic layer deposition as an optical biosensor platform for the detection of grapevine virus A-type proteins. *Biosens. Bioelectron.* **92**, 763 (2017).
85. **M. Dominik, A. Lesniewski, M. Janczuk, J. Niedziolka-Joensson, M. Holdynski, L. Wachnicki, M. Godlewski, W.J. Bock, and M. Smietana**: Titanium oxide thin films obtained with physical and chemical vapour deposition methods for optical biosensing purposes. *Biosens. Bioelectron.* **93**, 102 (2017).
86. **I.S. Wang, Y.T. Lin, C.H. Huang, T.F. Lu, C.E. Lue, P. Yang, D.G. Pijanswska, C.M. Yang, J.C. Wang, J.S. Yu, Y.S. Chang, C. Chou, and C.S. Lai**: Immobilization of enzyme and antibody on ALD-$HfO_2$-EIS structure by $NH_3$ plasma treatment. *Nanoscale Res. Lett.* **7**, 179 (2012).
87. **M. Lee, N. Zine, A. Baraket, M. Zabala, F. Campabadal, R. Caruso, M.G. Trivella, N. Jaffrezic-Renault, and A. Errachid**: A novel biosensor based on hafnium oxide: Application for early stage detection of human interleukin-10. *Sens. Actuators, B Actuat. B-Chem.* **175**, 201 (2012).
88. **S. Xie, S.I. Choi, N. Lu, L.T. Roling, J.A. Herron, L. Zhang, J. Park, J.G. Wang, M.J. Kim, Z.X. Xie, M. Mavrikakis, and Y. Xia**: Atomic layer-by-layer deposition of Pt on Pd nanocubes for catalysts with enhanced activity and durability toward oxygen reduction. *Nano Lett.* **14**, 3570 (2014).
89. **P.H. Mayrhofer, C. Mitterer, L. Hultman, and H. Clemens**: Microstructural design of hard coatings. *Prog. Mater. Sci.* **51**, 1032 (2006).
90. **C. Marichy, M. Bechelany, and N. Pinna**: Atomic layer deposition of nanostructured materials for energy and environmental applications. *Adv. Mater.* **24**, 1017 (2012).
91. **B. Zhu, X. Wu, W.J. Liu, H-L. Lu, D.W. Zhang, Z. Fan, and S.J. Ding**: High-performance on-chip supercapacitors based on mesoporous silicon coated with ultrathin atomic layer-deposited $In_2O_3$ films. *ACS Appl. Mater. Interfaces* **11**, 747 (2019).
92. **A. Purniawan, G. Pandraud, T.S.Y. Moh, A. Marthen, K.A. Vakalopoulos, P.J. French, and P.M. Sarro**: Fabrication and optical measurements of a $TiO_2$-ALD evanescent waveguide sensor. *Sens. Actuators, A* **188**, 127 (2012).
93. **B. Dunn, H. Kamath, and J.M. Tarascon**: Electrical energy storage for the grid: A battery of choices. *Science* **334**, 928 (2011).
94. **B. Scrosati and J. Garche**: Lithium batteries: Status, prospects and future. *J. Power Sources* **195**, 2419 (2010).
95. **J.L. Wang, J. Yang, C.R. Wan, K. Du, J.Y. Xie, and N.X. Xu**: Sulfur composite cathode materials for rechargeable lithium batteries. *Adv. Funct. Mater.* **13**, 487 (2003).
96. **D. Kundu, E. Talaie, V. Duffort, and L.F. Nazar**: The emerging chemistry of sodium ion batteries for electrochemical energy storage. *Angew. Chem., Int. Ed.* **54**, 3431 (2015).
97. **J. Fu, Z.P. Cano, M.G. Park, A. Yu, M. Fowler, and Z. Chen**: Electrically rechargeable zinc-air batteries: Progress, challenges, and perspectives. *Adv. Mater.* **29**, 1604685 (2017).
98. **S.Y. Lang, R.J. Xiao, L. Gu, Y.G. Guo, R. Wen, and L.J. Wan**: Interfacial mechanism in lithium–sulfur batteries: How salts mediate the structure evolution and dynamics. *J. Am. Chem. Soc.* **140**, 8147 (2018).
99. **N. Nitta, F. Wu, J.T. Lee, and G. Yushin**: Li-ion battery materials: Present and future. *Mater. Today* **18**, 252 (2015).

100. **Z.P. Cano, D. Banham, S. Ye, A. Hintennach, J. Lu, M. Fowler, and Z.W. Chen**: Batteries and fuel cells for emerging electric vehicle markets. *Nat. Energy* **3**, 279 (2018).

101. **M.Q. Snyder, S.A. Trebukhova, B. Ravdel, M.C. Wheeler, J. DiCarlo, C.P. Tripp, and W.J. Desisto**: Synthesis and characterization of atomic layer deposited titanium nitride thin films on lithium titanate spinel powder as a lithium-ion battery anode. *J. Power Sources* **165**, 379 (2007).

102. **D.T. Ma, Y.L. Li, J.B. Yang, H.W. Mi, S. Luo, L.B. Deng, C.Y. Yan, P.X. Zhang, Z.Q. Lin, X.Z. Ren, J.Q. Li, and H. Zhang**: Atomic layer deposition-enabled ultrastable freestanding carbon-selenium cathodes with high mass loading for sodium–selenium battery. *Nano Energy* **43**, 317 (2018).

103. **X. Han, Y. Gong, K. Fu, X. He, G.T. Hitz, J.Q. Dai, A. Pearse, B.Y. Liu, H. Wang, G. Rubloff, Y.F. Mo, V. Thangadurai, E.D. Wachsman, and L.B. Hu**: Negating interfacial impedance in garnet-based solid-state Li metal batteries. *Nat. Mater.* **16**, 572 (2017).

104. **J. Wolfenstine, J.L. Allen, J. Read, and J. Sakamoto**: Chemical stability of cubic $Li_7La_3Zr_2O_{12}$ with molten lithium at elevated temperature. *J. Mater. Sci.* **48**, 5846 (2013).

105. **S. Hy, Y.H. Chen, H.M. Cheng, C.J. Pan, J.H. Cheng, J. Rick, and B.J. Hwang**: Stabilizing nanosized Si anodes with the synergetic usage of atomic layer deposition and electrolyte additives for Li-ion batteries. *ACS Appl. Mater. Interfaces* **7**, 13801 (2015).

106. **E. Kazyak, K.H. Chen, K.N. Wood, A.L. Davis, T. Thompson, A.R. Bielinski, A.J. Sanchez, X. Wang, C.M. Wang, J. Sakamoto, and N.P. Dasgupta**: Atomic layer deposition of the solid electrolyte garnet $Li_7La_3Zr_2O_{12}$. *Chem. Mater.* **29**, 3785 (2017).

107. **C. Guan, X.L. Li, H. Yu, L. Mao, L.H. Wong, Q.Y. Yanc, and J. Wang**: A novel hollowed CoO-in-$CoSnO_3$ nanostructure with enhanced lithium storage capabilities. *Nanoscale* **6**, 13824 (2014).

108. **J. Jiang, J. Luo, J. Zhu, X. Huang, J. Liu, and T. Yu**: Diffusion-controlled evolution of core–shell nanowire arrays into integrated hybrid nanotube arrays for Li-ion batteries. *Nanoscale* **5**, 8105 (2013).

109. **M.P. Yu, J.S. Ma, H.Q. Song, A.J. Wang, F.Y. Tian, Y.S. Wang, H. Qiua, and R.M. Wang**: Atomic layer deposited $TiO_2$ on a nitrogen-doped graphene/sulfur electrode for high performance lithium-sulfur batteries. *Energy Environ. Sci.* **9**, 1495 (2016).

110. **B. Ahmed, D.H. Anjum, Y. Gogotsi, and H.N. Alshareef**: Atomic layer deposition of $SnO_2$ on MXene for Li-ion battery anodes. *Nano Energy* **34**, 249 (2017).

111. **M. Xie, X. Sun, S.M. George, C. Zhou, J. Lian, and Y. Zhou**: Amorphous Ultrathin $SnO_2$ Films by Atomic layer deposition on graphene network as highly stable anodes for lithium-ion batteries. *ACS Appl. Mater. Interfaces* **7**, 27735 (2015).

112. **Y.L. Li, Y.T. Zhao, G.S. Huang, B.R. Xu, B. Wang, R.B. Pan, C.L. Men, and Y.F. Mei**: ZnO nanomembrane/expanded graphite composite synthesized by atomic layer deposition as binder-free anode for lithium ion batteries. *ACS Appl. Mater. Interfaces* **9**, 38522 (2017).

113. **J.B. Goodenough and Y. Kim**: Challenges for rechargeable Li batteries. *Chem. Mater.* **22**, 587 (2010).

114. **D.T. Ma, Y.L. Li, J.B. Yang, H.W. Mi, S. Luo, L.B. Deng, C.Y. Yan, M. Rauf, P.X. Zhang, X.L. Sun, X.Z. Ren, J.Q. Li, and H. Zhang**: New strategy for polysulfide protection based on atomic layer deposition of $TiO_2$ onto ferroelectric-encapsulated cathode: Toward ultrastable free-standing room temperature sodium-sulfur batteries. *Adv. Funct. Mater.* **28**, 1705537 (2018).

115. **M.P. Yu, A.J. Wang, F.Y. Tian, H.Q. Song, Y.S. Wang, C. Li, J.D. Hongd, and G.Q. Shi**: Dual-protection of a graphene-sulfur composite by a compact graphene skin and an atomic layer deposited oxide coating for a lithium–sulfur battery. *Nanoscale* **7**, 5292 (2015).

116. **Y.W. Zhu, S. Murali, M.D. Stoller, K.J. Ganesh, W.W. Cai, P.J. Ferreira, A. Pirkle, R.M. Wallace, K.A. Cychosz, M. Thommes, D. Su, E.A. Stach, and R.S. Ruoff**: Carbon-based supercapacitors produced by activation of graphene. *Science* **332**, 1537 (2011).

117. **G.A. Snook, P. Kao, and A.S. Best**: Conducting-polymer-based supercapacitor devices and electrodes. *J. Power Sources* **196**, 1 (2011).

118. **P. Simon and Y. Gogotsi**: Materials for electrochemical capacitors. *Nat. Mater.* **7**, 845 (2008).

119. **A.G. Pandolfo and A.F. Hollenkamp**: Carbon properties and their role in supercapacitors. *J. Power Sources* **157**, 11 (2006).

120. **L. Wei, M. Sevilla, A.B. Fuertes, R. Mokaya, and G. Yushin**: Hydrothermal carbonization of abundant renewable natural organic chemicals for high-performance supercapacitor electrodes. *Adv. Energy Mater.* **1**, 356 (2011).

121. **X.L. Chen, L.B. Qiu, J. Ren, G.Z. Guan, H.J. Lin, Z.T. Zhang, P.N. Chen, Y.G. Wang, and H.S. Peng**: Novel electric double-layer capacitor with a coaxial fiber structure. *Adv. Mater.* **25**, 6436 (2013).

122. **S. Bose, T. Kuila, A.K. Mishra, R. Rajasekar, N.H. Kim, and J.H. Lee**: Carbon-based nanostructured materials and their composites as supercapacitor electrodes. *J. Mater. Chem.* **22**, 767 (2012).

123. **T. Sruthi and T. Kartick**: Route to achieving enhanced quantum capacitance in functionalized graphene based supercapacitor electrodes. *J. Phys.: Condens. Matter* **31**, 47 (2019).

124. **S.P. Liu and X.X. Pan**: An aqueous hybrid supercapacitor employing honeycomb-shaped $MoS_2$ nanosheets as anode. *J. Nanosci. Nanotechnol.* **20**, 1020 (2020).

125. **Y. Feng, Y. Li, W. Yang, and H. Huang**: Facile synthesis of nickel cobalt layered double hydroxide nanosheets intercalated with sulfate anion for high-performance supercapacitor. *J. Nanosci. Nanotechnol.* **20**, 1260 (2020).

126. **M. Fan, B. Ren, X. Yang, H. Yu, and L. Wang**: NiO@NiO and NiO@$Co_3O_4$ hollow core/shell composites for high-performance supercapacitor electrodes. *J. Nanosci. Nanotechnol.* **19**, 7785 (2019).

127. **C. Guan, X. Qian, X. Wang, Y. Cao, Q. Zhang, A. Li, and J. Wang**: Atomic layer deposition of $Co_3O_4$ on carbon nanotubes/carbon cloth for high-capacitance and ultrastable supercapacitor electrode. *Nanotechnology* **26**, 094001 (2015).

128. **J.S. Daubert, N.P. Lewis, H.N. Gotsch, J.Z. Mundy, D.N. Monroe, E.C. Dickey, M.D. Losego, and G.N. Parsons**: Effect of meso- and micro-porosity in carbon electrodes on atomic layer deposition of pseudocapacitive $V_2O_5$ for high performance supercapacitors. *Chem. Mater.* **27**, 6524 (2015).

129. **P. Ripka and M. Janosek**: Advances in magnetic field sensors. *IEEE Sens. J.* **10**, 1108 (2010).

130. **B. Lee, S. Roh, and J. Park**: Current status of micro- and nano-structured optical fiber sensors. *Opt. Fiber Technol.* **15**, 209 (2009).

131. **E.W. Hill, A. Vijayaragahvan, and K. Novoselov**: Graphene sensors. *IEEE Sens. J.* **11**, 3161 (2011).

132. **S.T. Han, H. Peng, Q. Sun, S. Venkatesh, K.S. Chung, S.C. Lau, Y. Zhou, and V.A.L. Roy**: An overview of the development of flexible sensors. *Adv. Mater.* **29**, 1700375 (2017).

133. **D. Zhang, K. Zhang, Y.L. Yao, X.H. Xia, and H.Y. Chen**: Multilayer assembly of prussian blue nanoclusters and enzyme-immobilized poly(toluidine blue) films and its application in glucose biosensor construction. *Langmuir* **20**, 7303 (2004).

134. **M. Chikae, T. Fukuda, K. Kerman, K. Idegami, Y. Miura, and E. Tamiya**: Amyloid-beta detection with saccharide immobilized gold nanoparticle on carbon electrode. *Bioelectrochemistry* **74**, 118 (2008).

135. **T. Choi, S.H. Kim, C.W. Lee, H. Kim, S-K. Choi, S-H. Kim, E. Kim, J. Park, and H. Kim**: Synthesis of carbon nanotube-nickel nanocomposites using atomic layer deposition for high-performance non-enzymatic glucose sensing. *Biosens. Bioelectron.* **63**, 325 (2015).

136. **C. Zhang, B. Huang, L. Qian, S. Yuan, S. Wang, and R. Chen**: Electrochemical biosensor based on nanoporous Au/CoO core–shell material with synergistic catalysis. *ChemPhysChem* **17**, 98 (2016).

137. **L. Wu, G. Wan, S. Shi, Z. He, X. Xu, Y. Tang, C. Hao, and G. Wang**: Atomic layer deposition-assisted growth of CuAl LDH on carbon fiber as a peroxidase mimic for colorimetric determination of $H_2O_2$ and glucose. *New J. Chem.* **43**, 5826 (2019).

138. **H. Cha, J. Lee, L.R. Jordan, S.H. Lee, S.H. Oh, H.J. Kim, J. Park, S. Hong, and H. Jeon**: Surface passivation of a photonic crystal band-edge laser by atomic layer deposition of $SiO_2$ and its application for biosensing. *Nanoscale* **7**, 3565 (2015).

139. **C. Wang, Q. Fu, X. Wang, D. Kong, Q. Sheng, Y. Wang, Q. Chen, and J. Xue**: Atomic layer deposition modified track-etched conical nanochannels for protein sensing. *Anal. Chem.* **87**, 8227 (2015).

140. **A. Purniawan, P.J. French, G. Pandraud, and P.M. Sarro**: $TiO_2$ ALD nanolayer as evanescent waveguide for biomedical sensor. *Procedia Eng.* **5**, 1131 (2010).

141. **D.J. Comstock, S.T. Christensen, J.W. Elam, M.J. Pellin, and M.C. Hersam**: Tuning the composition and nanostructure of Pt/Ir films via anodized aluminum oxide templated atomic layer deposition. *Adv. Funct. Mater.* **20**, 3099 (2010).

142. **X. Du and S.M. George**: Thickness dependence of sensor response for CO gas sensing by tin oxide films grown using atomic layer deposition. *Sens. Actuators, B* **135**, 152 (2008).

143. **A.J. Niskanen, A. Varpula, M. Utriainen, G. Natarajan, D.C. Cameron, S. Novikov, V.M. Airaksinen, J. Sinkkonen, and S. Franssila**: Atomic layer deposition of tin dioxide sensing film in microhotplate gas sensors. *Sens. Actuators, B* **148**, 227 (2010).

144. **D.J. Yun, G.H. Seo, W.H. Lee and S.M. Yoon**: Improvement in Sensing Responses to Ammonia Gas for Gas Sensors With Separately Designed Sensing Element Using ALD-Grown ZnO Nanoparticles and Read-Out Element of Top-Gate In-Ga-Zn-O Thin-Film Transistor *IEEE Transactions on Electron Devices* **64**, 2350 (2017).

145. **C. Han, X. Li, C. Shao, X. Li, J. Ma, X. Zhang, and Y. Liu**: Composition-controllable p-CuO/n-ZnO hollow nanofibers for high-performance $H_2S$ detection. *Sens. Actuators, B* **285**, 495 (2019).

146. **Y.T. Lin, C.S. Huang, L. Chow, J.M. Lan, C.M. Yang, L.B. Chang, and C.S. Lai**: Light-immune pH sensor with SiC-based electrolyte-insulator-semiconductor structure. *Appl. Phys. Express* **6**, 127002 (2013).

147. **M.H. Jakob, S. Gutsch, C. Chatelle, A. Krishnaraja, J. Fahlteich, W. Weber, and M. Zacharias**: Flexible thin film pH sensor based on low-temperature atomic layer deposition. *Phys. Status. Solidi Rapid Res. Lett.* **11**, 1700123 (2017).

148. **L. Wang, L. Li, T. Zhang, X. Liu, and J.P. Ao**: Enhanced pH sensitivity of AlGaN/GaN ion-sensitive field effect transistor with $Al_2O_3$ synthesized by atomic layer deposition. *Appl. Surf. Sci.* **427**, 1199 (2018).

149. **Q.L. Guo, Y.T. Zhao, G. Wang, D. Chen, H.N. Zhao, C.M. Jiang, G.S. Huang, Z.F. Di, and Y.F. Mei**: Sponge-templated production of ultra-thin ZnO nanosheets for printed ultraviolet photodetectors. *Appl. Phy. Lett.* **115**, 122106 (2019).

150. **Y.T. Zhao, G.S. Huang, Y.L. Li, R. Edy, P. Gao, H. Tang, Z. Bao, and Y.F. Mei**: Three-dimensional carbon/ZnO nanomembrane foam as an anode for lithium-ion battery with long-life and high areal capacity. *J. Mater. Chem. A* **6**, 7227 (2018).